

Self-Healing Coatings for Steel-Reinforced Infrastructure

A Major Qualifying Project
Submitted to the Faculty of
Worcester Polytechnic Institute
in partial fulfillment of the requirements for the
Degree in Bachelor of Science
in
Chemical Engineering
Civil Engineering
By

Yixi Chen

Nicholas Rice

Nicholas Smith

Chris Xia

Date: 3/25/15

Project Advisor:

Amy Peterson

Aaron Sakulich

This report represents work of WPI undergraduate students submitted to the faculty as evidence of a degree requirement. WPI routinely publishes these reports on its web site without editorial or peer review. For more information about the projects program at WPI, see <http://www.wpi.edu/Academics/Projects>.

Abstract

Infrastructure maintenance costs billions of dollars every year and inconveniences millions of people every day. One of the primary causes of the damage and deterioration of infrastructure is the corrosion of steel reinforcement in concrete. A popular option for the protection for steel reinforcement is epoxy coating, but when damaged this coating becomes ineffective. A possible improvement to this system involves incorporating self-healing agents into the epoxy coating, allowing damage to be automatically repaired, extending the life of the rebar and therefore the structure. This paper presents the results of experimentation conducted with tung oil, a possible self-healing agent. Micro-encapsulated tung oil was incorporated into a two-part epoxy. The resulting coating was applied to steel rebar and subjected to a number of tests, including accelerated corrosion testing. This corrosion testing formed the backbone of the results, showing that the experimental coatings with microcapsules exhibited significantly longer lifespans than samples with regular epoxy coatings when subjected to a controlled corrosive environment. These results indicate a promising future for self-healing coatings and many opportunities for continued research and development.

Table of Contents

Introduction.....	6
Background.....	7
Composite Design.....	7
Corrosion and Deterioration of Concrete Structures	7
Corrosion Prevention Methods	8
Self-Healing Coatings.....	10
Literature Review.....	11
Concrete Mix Design	11
Epoxy Coatings.....	11
Self-Healing Coatings.....	11
Benzotriazole Encapsulated Self-Healing Coatings	12
Bismaleimide Encapsulated Self-Healing Coatings	12
Drying Oil Encapsulated Self-Healing Coatings	13
Experimental.....	14
Synthesis of Microcapsules.....	14
Encapsulation of Tung Oil	14
Encapsulation of 2-methylbenzothiazole	15
Microcapsule Characterization	17
Preparation of Self-healing Coating.....	17
Preparation of Coated Rebar.....	17
Concrete Mix Design	18
Compression Testing	18
Accelerated Corrosion Testing	21
Pullout Testing.....	22
Results and Discussion	24
Synthesis of Microcapsules.....	24
Mechanical Stirrer verses Magnetic Stirrer	24
Encapsulation of Tung Oil	24
Encapsulation of 2-methylbenzothiazole	26
Preparation of Self-healing Coating.....	29
Effect of Microcapsules on Epoxy Curing.....	29

Coating Thicknesses	30
Self-healing Ability.....	30
Concrete Mix Design	32
Sieve Analysis.....	32
Compression Testing	33
Pullout Testing.....	34
Accelerated Corrosion Testing	35
Conclusions.....	38
Appendix A.....	39
Synthesis of Microcapsules.....	39
Tung oil-microcapsules used in accelerated corrosion test:	39
Tung Oil- microcapsules used in thickness test:.....	41
2-Methylbenzothiazole - failed attempt:.....	43
Appendix B	44
Quality Test.....	44
Sieve Analysis.....	44
Pullout Testing	45
Compression Test.....	47
Thickness Test	49
Appendix C	50
Accelerated Corrosion Test.....	50
Regular Coating Trial 1:	50
Civil Engineering Design Statement.....	51
Professional Licensure Statement	52
References.....	53

Table of Figures

Figure 1: Setup for microcapsule synthesis	15
Figure 2: The cut made on rebar coatings	18
Figure 3: The concrete cube for 1-day testing	20
Figure 4: Compression testing for 28-day concrete cube	21
Figure 5: Setup for accelerated corrosion testing	22
Figure 6: Setup for pullout testing	23
Figure 7: Appearance of synthesized microcapsules containing tung oil. The images of the whole batch of microcapsules in a Petri dish (left) and some microcapsules (right)	24
Figure 8: SEM images of (a) synthesized microcapsules containing tung oil; (b) the detail of a crack	25
Figure 9: TGA curve of synthesized microcapsules containing tung oil	26
Figure 10: Encapsulation of 2-methylbenzothiazole by Latnikova <i>et al.</i> (left) and encapsulation of 2-methylbenzothiazole by MQP group (right)	27
Figure 11: TGA graph of 2-methylbenzothiazole microcapsules by Latnikova <i>et al.</i> (Top) and experimental TGA graph (bottom)	28
Figure 12: Outside diameter of coated rebars	30
Figure 13: Optical microscope images of tung oil bleeding out of a microcapsule under (a) low, (b) medium, and (c) high exposure (10 wt.%, 5 days after damage)	31
Figure 14: Optical microscope images of cuts made on samples. (a) A cut made on unmodified epoxy coating; (b) a cut made after 5 days on the sample with 20 wt.% microcapsules; (c) a cut made immediately on the sample with 20 wt.% microcapsules; (d) a close up image of an microcapsule (5 days)	32
Figure 15: Sieve analysis results of aggregate	33
Figure 16: Graph of the peak strengths on various days of the compression tests	33
Figure 17: Graph of the peak strengths on various days of the pullout test	34
Figure 18: A broken sample by pullout testing coated with self-healing coating with 20 wt.% microcapsules	35
Figure 19: Failure time for accelerated corrosion test	36

Figure 20: Voltage with respect to time for 20 wt.% damaged in accelerated corrosion test	36
Figure 21: One of the corroded samples for unmodified epoxy coating	37
Figure 22: SEM images of microcapsules containing tung oil from one of the batches ..	39
Figure 23: SEM images of microcapsules containing tung oil from a different batch	39
Figure 24: Size distribution of tung oil microcapsules	40
Figure 25: Thermalgravimetric Analysis of encapsulated tung oil over temperature	40
Figure 26: Thermalgravimetric Analysis of encapsulated tung oil over time	41
Figure 27: Size distribution of tung oil microcapsules	41
Figure 28: Thermalgravimetric Analysis of encapsulated tung oil over temperature	42
Figure 29: Comparison of the microcapsules size for the thickness test and the microcapsule size for the accelerated corrosion test.	42
Figure 30: Thermalgravimetric Analysis of the attempt to encapsulate 2-methylbenzothiazole over temperature.....	43
Figure 31: Thermalgravimetric Analysis of the attempt to encapsulate 2-methylbenzothiazole over time.....	43
Figure 32: Graduation Chart for comparison of industry standard and experimental aggregate	44
Figure 33: Table of percent passing industry standard and experimental aggregate	44
Figure 34: Table of the peak stresses of the pullout test.....	45
Figure 35: Pullout graphs of the uncoated samples	45
Figure 36: Pullout graphs of the regular coated samples	46
Figure 37: Pullout graphs of the 10 wt.% tung oil EC samples	46
Figure 38: Pullout graphs of the 20 wt.% tung oil EC samples	47
Figure 39: Compression test of day 1 peak strengths	47
Figure 40: Compression test of day 7 peak strengths	48
Figure 41: Compression test of day 28 peak strengths	48
Figure 42: Statistics for coating thickness measurement.....	49
Figure 43: Average for coating thickness measurement.....	49
Figure 44: Graph of current with time of regular coating undamaged	50
Figure 45: Graph of current with time of regular coating damaged	50

Introduction

According to the American Society of Civil Engineers (ASCE), which provides a rating of the various aspects of the nation's infrastructure every four years, the United States is currently suffering from the rapid deterioration of its infrastructure, with many concrete structures falling into poor condition and maintenance projects showing very little overall improvement [1]. This is a significant problem, with repairs and replacements costing hundreds of billions of dollars in total [2], causing delays to hundreds of millions of trips daily [1] and impacting the environment significantly.

Corrosion of the reinforcing steel bar in concrete, called rebar, is one of the leading causes of infrastructure deterioration. Rebar is included in nearly every concrete structure and is typically protected against external factors that would cause rusting by a thin epoxy coating. If this coating is damaged, however, water and corrosive agents can come in contact with the rebar and cause it to rust more quickly. The corrosion causes rebar to greatly increase its volume, producing internal stresses in the concrete which break it apart from within. Therefore, improvements in corrosion inhibition of rebar are of significant importance in prolonging the service life of reinforced concrete structures.

In order to achieve the objective of preventing rebar corrosion and subsequent reinforced concrete deterioration, self-healing coatings for rebar were investigated in this project. Self-healing coatings are capable of repairing themselves after damage and therefore are a significant improvement over unmodified epoxy coatings. Even though damage usually occurs during the initial construction, it may happen at any time throughout the life of the structure. This project reports the first use of self-healing coatings for steel-reinforced concrete. Specifically, tung oil was encapsulated in poly(urea-formaldehyde), embedded into epoxy resin, and then applied to rebar.

Background

Composite Design

Rebar is added to concrete structures in order to take advantage of both the properties of the concrete and the rebar [16]. Concrete has a high compressive strength but a low tensile strength. When coupled with rebar, the composite structure makes use of the rebar's strength in tension while relying on the concrete exclusively for its compressive strength [16]. For this reason it is important that a strong shear bond is formed between the reinforcement and the concrete so that the rebar does not separate from the concrete when the system is put into tension [10].

Rebar has grooves or ridges in it to facilitate a solid bond between the reinforcement and the concrete [17, 18]. However, the addition of coatings to rebar changes the interface, which may change the shear bond strength between the rebar and concrete [10]. If a coating is too thick, ridges in the rebar will be diminished, which can decrease the pullout strength. Depending on the shear strength and adhesive qualities of the coating, there is potential for the coating to delaminate from the rebar, the concrete, or both when the rebar is placed under stress [18]. If any material or interface fails when transferring the forces between the concrete and steel, then the entire system may fail.

Corrosion and Deterioration of Concrete Structures

The deterioration of concrete structures can be attributed to many factors, including overloading, metal fatigue, and natural disasters. The corrosion of rebar in concrete, however, is one of the leading causes. Steel is chosen for its ease of placement, wide availability, and its tensile and flexural strength. The major problem with most types of steel rebar is that steel rusts [3]. Steel starts off as iron (Fe) smelted in a high-temperature process to incorporate carbon atoms [4]. The carbon greatly increases the

strength of the iron but simultaneously gives steel a net positive charge [5]. This net positive charge allows steel to react with anions, forming iron(II) hydroxide ($\text{Fe}(\text{OH})_2$) and iron(III) oxide (Fe_2O_3) [5]. When the steel oxidizes, it expands to a volume roughly six to eight times larger, causing tensile stresses in the concrete that eventually lead to spalling and cracking [6].

Due to the natural alkaline environment of concrete, embedded steel forms a stable oxide layer on its surface, sealing it off from further corrosion [7]. Although the steel underneath will still corrode, further oxidation will happen at a much slower pace than would normally occur [7]. This balance is upset, however, when aggressive agents are present. Concrete is porous and therefore salts may be carried by water through even undamaged concrete and come in contact with the metal surface. The presence of these salt ions causes the steel to corrode much more quickly.

Concrete also tends to undergo degradation due to the environment. The primary ingredients in concrete are aggregate, such as sand or gravel, and cement paste. Cement paste is the adhesive that holds together the aggregate together, and it is more susceptible to deterioration than most aggregates. As the cement in concrete degrades, cracks form and pieces of aggregate become loose. These cracks allow water and air to easily reach the rebar within the structure. Water reaching the structure's reinforcement will then cause the rebar to degrade at a faster rate. This rapid corrosion then leads to the need for more repairs or premature replacements of structures.

Corrosion Prevention Methods

Many approaches have been developed to prevent rebar from corroding. One widely used method is to coat rebar with epoxy. The epoxy coating prevents moisture, oxygen, and salts from coming in contact with the rebar. This method is relatively

inexpensive and easy to apply, but fails to protect rebar in concrete when the epoxy coating is damaged or cracked. Weak physical bonding between epoxy and rebar is another hindrance to effectively protecting concrete reinforcement [8]. Previously, hexavalent chromium was commonly added to epoxy coating because it served as a good anticorrosive additive to paints, primers, and other coatings, but it is known to be a carcinogen and increase the risk of lung cancer [9, 10]. Therefore, investigations in safer anticorrosive substances have been suggested [11, 12].

Another method of corrosion inhibition is to use stainless steel for rebar. Stainless steel is significantly less prone to corrosion than carbon steel, and thus prolongs the service life of reinforced concrete [13]. However, stainless steel is not widely incorporated into concrete structures due to its high cost, about 2.5 to 4 times the cost of carbon steel [14]. Using stainless steel for all rebar would significantly raise the capital cost of a project.

Galvanic protection, also called cathodic protection, is another effective method of protecting rebar in concrete. There are two distinct approaches to cathodic protection: passive galvanic protection and active systems. Passive galvanic protection involves attaching a sacrificial metal, such as zinc or aluminum, in order to reduce corrosion of rebar electrochemically [15]. This method is commonly used in concrete structures for pipelines, storage tanks, and offshore platforms. Active systems involve the implementation of an external current and are only used for very large applications such as ship hulls [15]. Although galvanic protection can significantly increase the life of reinforcement and the concrete structure, it is more expensive than either carbon steel or epoxy coated rebar.

Self-Healing Coatings

Self-healing coatings are an exciting technology capable of recovering their initial properties after being damaged. Conventional corrosion inhibiting coatings have reduced function when the coatings are damaged and the metal underneath is exposed to corrosive agents. For example, the epoxy coated rebar used today works well only when the coating is still intact. In contrast, self-healing coatings can continue to inhibit corrosion even after the material is damaged because the defects are automatically repaired, or “self-healed”. Therefore, introducing a corrosion inhibiting self-healing coating on rebar should greatly prolong the life of the steel reinforced concrete structure. This is a novel concept that has not yet been investigated.

Literature Review

Corrosion of metals is an electrochemical phenomenon that is unwanted in almost all situations, other than those in which the corrosion is intentionally used to produce a protective coating. The two primary approaches to inhibit corrosion in reinforced concrete structures involve either modifying the concrete or coating the rebar.

Concrete Mix Design

Significant research has been conducted regarding inhibiting corrosion through the manipulation of the concrete mix. In one example, Okba *et al.* investigated the resistive qualities of latex modified concrete (LMC), finding that across the board it provided better protection against corrosion than conventional concrete [19]. LMC is a variation of standard concrete containing a latex polymer that works with the cement as a binding agent [20]. LMC's anti-corrosive abilities result from its increased waterproofness and chemical resistance to some salts over regular concrete [20]. Unfortunately, LMC is more expensive than conventional concrete so further investigation is required to determine the most efficient use of LMC as rebar cover [19].

Epoxy Coatings

Applying a coating on rebar is another method to protect it from corrosion. Epoxy coatings applied to rebar are widely used for their ability to prevent or limit water and corrosive agents from reaching the rebar [20]. In one study, slabs containing uncoated steel were compared to slabs containing epoxy coated steel and both were subjected to long-term corrosion testing. The results showed that epoxy coatings prevented significant corrosion for 9 years as opposed to the 1.5 years of uncoated steel [21].

Self-Healing Coatings

Self-healing mechanisms, while not previously investigated for application to concrete-encased rebar coatings, have been shown to repair damage in other materials,

including polymer coatings for metals. There are many healing mechanisms available for self-healing coatings when the goal is to prevent corrosion, and several were researched as potential subjects for this study. The healing agents must be contained somehow in order to incorporate them in epoxy coatings, which can be done using microcapsules. Many microencapsulation methods for self-healing coatings have been based on Brown's *et al.* encapsulation procedure of dicyclopentadiene (DCPD) in poly(urea-formaldehyde) [22]. Incorporating a microencapsulated self-healing agent into the epoxy resin may greatly improve and prolong the life of rebar.

Benzotriazole Encapsulated Self-Healing Coatings

Benzotriazole can be incorporated into a coating used to protect metals from oxidation. It is known to be one of the top corrosion inhibitors of copper and its alloys [23]. Benzotriazole is commonly used with other substances, such as manganese(III) oxide ($\alpha\text{-Mn}_2\text{O}_3$), to improve the reaction of benzotriazole with copper that produces a corrosion barrier [24]. Micro- or nanocontainers can be loaded with benzotriazole allowing it to be easily incorporated into a coating. Borisova *et al.* and Abdullayev *et al.* successfully loaded it in nanocontainers to inhibit the corrosion of an aluminum alloy [25, 26]. Additionally, Latnikova *et al.* encapsulated 2-methylbenzothiazole (MeBT), a corrosion inhibitor similar to benzotriazole, in polyurea [27]. Microcapsules filled with MeBT could potentially be used for self-healing epoxy coatings for rebar.

Bismaleimide Encapsulated Self-Healing Coatings

Bismaleimide solutions have also been encapsulated and incorporated into appropriate epoxy thermosets to produce self-healing coatings. Bismaleimides reacts with furans thermoreversibly through the Diels-Alder reaction. Peterson *et al.* extensively investigated the properties and performance of a furan-functionalized epoxy-amine

thermoset that could be healed with a bismaleimide solution [28-31]. In this system the solvent swells and makes the polymer rubbery when the polymer is damaged and microcapsules rupture. When bismaleimides reacts with furans within the polymer network, they form covalent bonds across a crack. Pratama *et al.* developed a method to encapsulate multimaleimide solutions with poly(urea-formaldehyde) (pUF) microcapsules [32, 33]. Therefore, furan-functionalized epoxy-amine thermosets could potentially be used as self-healing coatings for rebar.

Drying Oil Encapsulated Self-Healing Coatings

Another set of potentially effective healing agents are drying oils including linseed oil, tung oil, and walnut oil. When drying oils are exposed to air for a period of time, they polymerize and form a hard waterproof film. Because of this property, drying oils have been widely used for coatings in paintings and varnishes for centuries. Scientists have extensively investigated the encapsulation of linseed oil and tung oil in pUF microcapsules [34-38]. Samadzadeh *et al.* was the first to successfully synthesized drying oil-encapsulated self-healing coatings [36]. These pUF microcapsules filled with drying oils have a rough shell allowing good adhesion with the epoxy matrix [36]. The size of the microcapsules can be easily controlled by the rate of agitation [35]. The relative kinetics between polymerization of drying oils and rust formation on concrete rebar has never been investigated, making drying oil encapsulated self-healing coatings a prime subject for research and testing.

Experimental

Synthesis of Microcapsules

Encapsulation of Tung Oil

Urea, ammonium chloride, resorcinol, formaldehyde, and tung oil were purchased from Sigma-Aldrich. Ethyl maleic anhydride (EMA) was purchased from Vertellus. All chemicals were used without any purification. ULTRA-TURRAX high-speed homogenizer (IKA Werke, Staufen, Germany) was used for mixing the solution.

The procedure used for encapsulating tung oil was based on the method described by Samadzadeh *et al.* [36]. The encapsulation began with an oil-in-water emulsion to which the following components were added: ethyl maleic anhydride (EMA) solution as a surfactant, resorcinol to stabilize the solution, ammonium chloride to provide a pH buffer, and urea reacting with formaldehyde to form the polymer shells.

At room temperature, 200 mL of deionized water, 25 mL of 2.5 wt.% EMA solution, 0.5 g of resorcinol, 0.5 g of ammonium chloride, and 5 g of urea were mixed fully in a 500 mL beaker. Following this, the pH of the solution was adjusted from 2.7 to 3.5 using dilute sodium hydroxide solution in order to control the morphology of the polymer shells. This solution was placed into a room temperature water bath and kept stirring at 400 rpm as 50 mL of tung oil was slowly added into the solution. The resulting mixture was mechanically stirred at 400 rpm for 10 minutes to form a stabilized emulsion, after which 13 g of 37 wt.% formaldehyde solution was added. The temperature of the solution was raised to 60 °C for 4 hours at 400 rpm to facilitate the polymerization reaction between urea and formaldehyde. The solution was then removed from the oil bath and stirred as it cooled to room temperature over 6 hours. To extract the microcapsules, the mixture was vacuum filtered with coarse filter paper, then washed twice with deionized water and twice with acetone, respectively. Finally, the

microcapsules were air-dried for 48 hours before they could be used. The setup was as shown below.

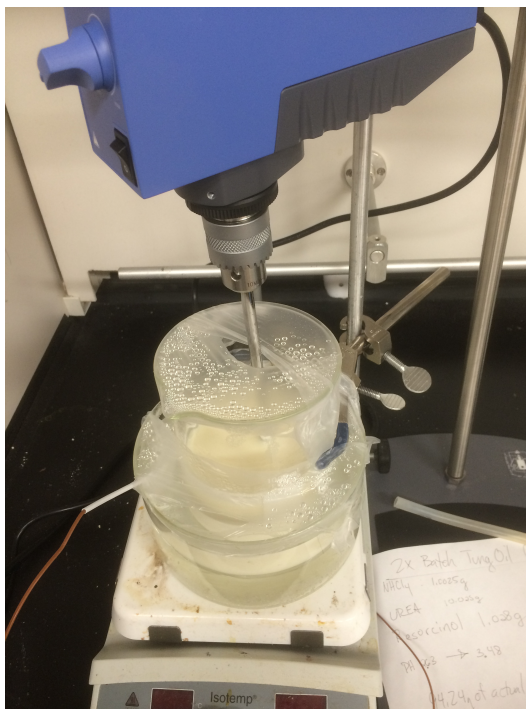


Figure 1: Setup for microcapsule synthesis

Encapsulation of 2-methylbenzothiazole

Both poly[(phenyl isocyanate)-co-formaldehyde] (isocyanate pre-polymer, number of reactive groups per molecule~3.0, MW~375) and poly(vinyl alcohol) (PVA, MW~9,000-10,000, 80% hydrolyzed) were purchased from Sigma-Aldrich. 2-methylbenzothiazole was purchased from Fischer Scientific, ethylenediamine was purchased from Alfa Aesar, and tetraethylenepentamine (TEPA) was purchased from Acros Organics. All chemicals were used without any purification.

Two different methods to encapsulate 2-methylbenzothiazole were attempted. The first method, which has not been previously reported in the literature, used the same procedure as the tung oil encapsulation while the other method was based on the procedure previously reported by Latnikova *et al.* [27].

The tung oil method used to encapsulate 2-methylbenzothiazole utilized the same chemicals and proportional amounts as in the procedure to encapsulate tung oil. At room temperature, 40 mL of deionized water, 5 mL of 2.5 wt.% EMA solution, 0.1 g of resorcinol, 0.1 g of ammonium chloride, and 1 g of urea were mixed fully in a 500 mL beaker. Once the solids were completely dissolved, the solution was adjusted to a pH of 3.5 using dilute sodium hydroxide. This was placed into a room temperature water bath and kept stirring at 400 rpm as 5 mL of 2-methylbenzothiazole was slowly added to the solution. The resulting mixture was mechanically stirred at 400 rpm for 10 minutes to form a stabilized emulsion, after which 2.6 g of 37 wt.% formaldehyde solution was added. The temperature of the solution was raised to 60 °C for 4 hours at 400 rpm to facilitate polymerization reaction. The resulting solution was filtered using vacuum filtration and rinsed twice with deionized water and twice with acetone.

The method from Latnikova *et al.* [27] took a completely different approach than the tung oil method. Instead of synthesizing a polymer in a solution, a prepolymer was used to encapsulate the healing agent. This method also asked for a homogenizer to emulsify the solution but it was unavailable in the laboratory. Therefore, a mechanical stirrer was used instead and the chemical amounts used were tripled to allow for proper mixing.

A solution of 900 mg of isocyanate prepolymer and 2100 mg of 2-methylbenzothiazole was emulsified in a 10mL of 2 wt.% of aqueous poly-(vinyl alcohol) (PVA) using a 4 impeller mechanical stirrer at 400 rpm. While the solution was emulsifying for about 18 minutes, another solution consisting 3.3g of ethylenediamine (EDA), 11.4 g of tetraethylenepentamine (TEPA), and 30 mL of water was prepared.

This solution was then added to the emulsified solution under constant stirring for about 10 minutes [27]. The combined solution was covered with Parafilm and allowed to react for 10 hours at room temperature. To extract the product, the solution was vacuum filtered with coarse filter paper, then washed twice with deionized water and twice with acetone. The particles were air-dried for 48 hours under the fume hood.

Microcapsule Characterization

Microcapsules were characterized using two methods. First, the microcapsules were imaged with scanning electron microscopy (SEM) to determine the morphology and the size distribution of microcapsules. Thermogravimetric analysis (TGA) was also conducted to determine the thermal stability of microcapsules.

Preparation of Self-healing Coating

To make the experimental epoxy coating, microcapsules containing tung oil and a 2-part epoxy coating (Super Glaze, Rust-Oleum Parks) were used. Two different coatings were synthesized: coatings with 10 wt.% and 20 wt.% tung oil microcapsules. Minimizing air bubbles in the epoxy resin microcapsule mixture was necessary to prevent void formation in the coating. Therefore, a planetary centrifugal mixer (Thinky Mixer) was utilized to mix the microcapsules and epoxy. All the mixing in Thinky was performed at 200 rpm for 2 minutes and degassed at 400 rpm for 30 seconds in order to prevent microcapsule from rupture.

Preparation of Coated Rebar

12'' rebar for lollipop samples and 36'' rebar for pullout samples were cleaned and dip-coated. The coatings were then allowed to cure for 72 hours at room temperature before being encased in a concrete sample. Damaged rebar samples were made by using a utility knife to make a 3-inch cut in the unmodified epoxy coating as well as the experimental coatings. This cut was 1-inch from the bottom of the rebar, as shown below.



Figure 2: The cut made on rebar coatings

In addition to the samples for the accelerated corrosion test, another set of samples was prepared to measure the thickness of the coatings. Once the coatings were fully cured, a caliper was used to measure the outer diameter of the coated rebar.

Concrete Mix Design

The concrete mix that was used was for a standard mortar and specified that 45 vol% of the dry ingredients must be cement and for the other 55 vol% to be fine aggregate. A 0.3 water-to-cement ratio was determined to be adequate to make the samples easily workable but also sufficiently strong.

Following these ratios for our typical 1 kg batch, 550 g of fine aggregate, 104 g of water, and 346 g of portland cement were added. Batches of this size were made in order to ensure the materials were sufficiently mixed together into one homogeneous cement mix.

Compression Testing

The mix design also underwent compression testing before it was used in accelerated corrosion testing to ensure the compression strength matched standard

industry values. Any significant variation would have indicated a problem with the process used to mix, pour, or cure the concrete. To perform this testing, a commercial grade mixer was used to combine the dry aggregate and portland cement for 2 minutes before slowly adding water to the mix and mixing for an additional 4 minutes. This mix was then allowed to sit for 1 minute before being turned by hand and then placed into molds.

Prior to the mix being placed into the cube molds, the molds were assembled and lightly wiped down with WD40 as a release agent to help remove the molds later. The cube molds were then filled 1/3 of the way and rodded 12 times each. They were filled a further 1/3 and rodded 12 times each again before being filled the remaining 1/3 and then being rodded a final 12 times each. This process helps remove air bubbles from the concrete mix. Large air voids could cause samples to have imperfections, which lead to underperformance in testing. The entire mold was then placed into a sealed plastic bag and placed in the curing room. The bag was placed on the sample to keep the relative moisture content in the bag stable for the initial curing period. Twenty-four hours after pouring, the cubes were then demolded and placed back into the curing room without the plastic bag until they had cured for the specified amount of time for testing. One of the samples was shown as below.

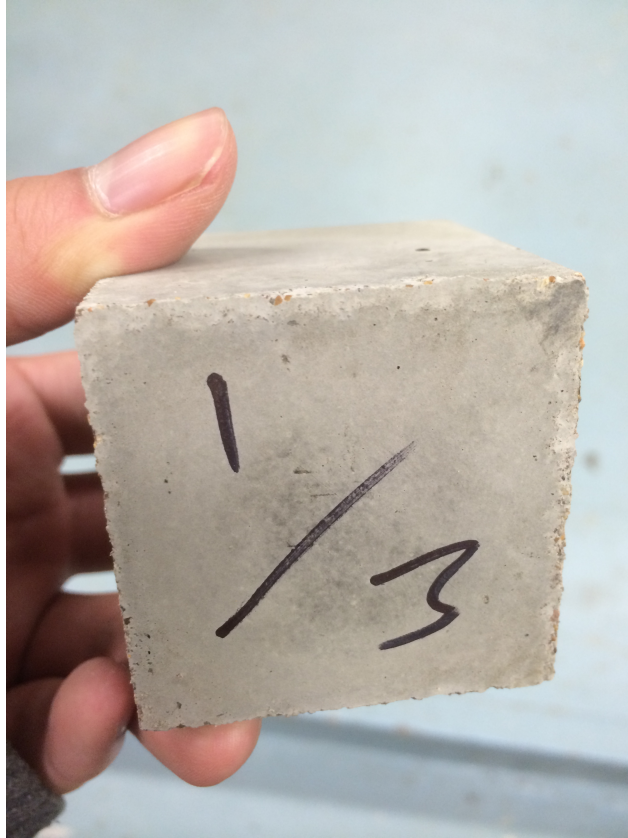


Figure 3: The concrete cube for 1-day testing

The compression test cubes were tested after 1 day, 7 days, and 28 days of curing in order to obtain representative graphs of the development of the mix designs strength. This testing was performed with a Tinius Olson Universal Testing Machine.

Prior to testing, each of the samples was measured and weighed. The dimensions of the samples were then put into the program that runs the tester in order to accurately calculate the stresses the cubes underwent. The samples were each individually placed in the center of the base of the tester and the upper powerhead was then lowered until it was 1/4" from the top of the sample. The powerhead was then brought down with the fine adjustment until it was just barely making contact with the top of the cube. The cube was then ready to undergo the testing procedure.

Specimens were compressed at a load rate of 2000 pounds per minute until they failed, as shown below. The 3 samples for each cure period were then analyzed to determine whether the strength of the mix was adequate for use in all of our samples.



Figure 4: Compression testing for a 28-day concrete cube

Accelerated Corrosion Testing

The accelerated corrosion testing was based on the procedure previously used by Ahmad [39]. The 3” diameter by 6” tall cylindrical concrete samples were prepared with rebar partially encased in them. The 1’ long rebar was suspended 0.75” from the bottom of the mold and extended out of the top of the concrete. Sets of the rebar were coated with one of the four coating types being tested: no coating, unmodified epoxy coating, and epoxy coating mixed with 10 wt.% and 20 wt.% of microcapsules containing tung oil. These samples were submerged in a 5 wt.% sodium chloride (Alfa Aesar) solution with

the waterline just below the top of the concrete and the rebar extending upward. Two stainless steel plates were placed in the solution on opposite sides of each sample. 30-volt power supplies were used to apply a current through the system with the stainless steel plates attached to the negative leads and the rebar protruding from the sample attached to the positive lead. A data logging program tracked the current in the circuit at regular intervals, which allowed the determination when the first full crack forms in each sample. A spike in current was observed when a crack was initiated due to significant loss in electrical resistance. The setup was shown as below.



Figure 5: Setup for accelerated corrosion testing

Pullout Testing

The pullout testing was conducted based on standard laboratory practices. 3' long pieces of rebar were coated in each type of coating, then encased in 3" diameter by 6" tall

concrete cylinders. After full concrete curing, each cylinder was then placed in the universal testing machine with the rebar clamped and the concrete cylinder braced. The rebar was pulled away from the concrete at a uniform rate of 8000 pounds per minute until it broke from the concrete. The results of this test allowed determination of the effect of adding microcapsules to an epoxy coating on the pullout strength of rebar encased in concrete. The setup for pullout testing was shown as below.



Figure 6: Setup for pullout testing

Results and Discussion

Synthesis of Microcapsules

Mechanical Stirrer verses Magnetic Stirrer

It is critical to mix the solution evenly during the encapsulation process. In early studies a magnetic stirrer was used, resulting in numerous failed attempts to produce microcapsules. It was observed that synthesized microcapsules tended to aggregate, forming many polymer clumps and clogging the filter paper. Additionally, only shrunken or broken microcapsules were observed under SEM. All of these phenomena were caused by unevenly distributed drops of tung oil in the solution and a polymerization process that failed to occur evenly on the surface of the oil drops. However, when a mechanical stirrer was used for mixing the solution at the same stirring rate, the particles were discrete and easily filtered. Therefore, good mixing must be achieved in order to produce high-quality microcapsules.

Encapsulation of Tung Oil

Microcapsules containing tung oil were successfully synthesized. As shown in Figure 7 the product was discrete, slightly yellow particles, the shape of which could be easily observed with the naked eyes. It was also observed that a drop of yellow liquid came out when some of the microcapsules broke.

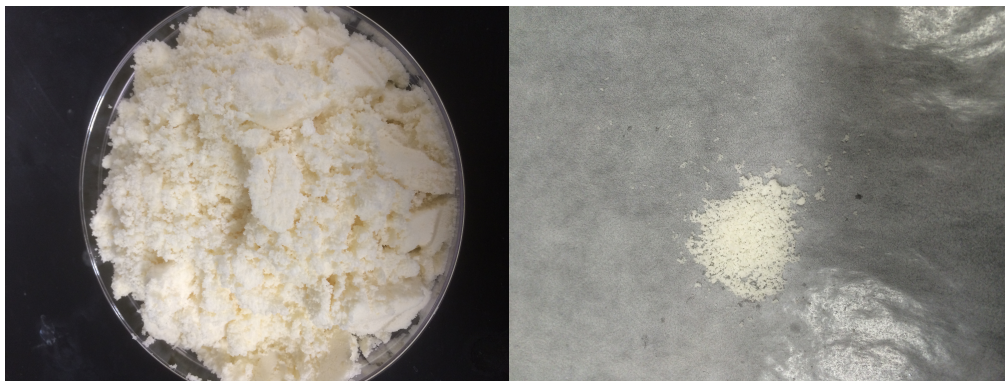


Figure 7: Appearance of synthesized microcapsules containing tung oil. The images of the whole batch of microcapsules in a Petri dish (left) and some microcapsules (right)

The synthesized microcapsules were imaged by SEM. As shown below in Figure 8, the microcapsules are spherical and have a rough shell, indicating that they will have good adhesion with epoxy coating. The average size of the microcapsules was determined using ImageJ to be around 300 μm . However, the size distribution of microcapsules used for the accelerated corrosion testing was broad and had multiple peaks, as a few batches of microcapsules synthesized at different times were combined, and the size distribution from each batch differed due to the lack of strict quality control during the microcapsules synthesis.

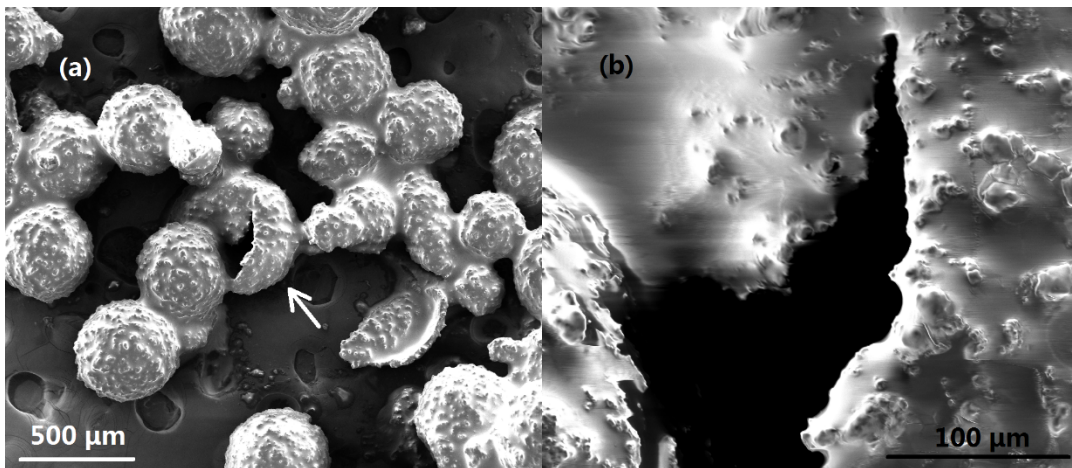


Figure 8: SEM images of (a) synthesized microcapsules containing tung oil; (b) the detail of a crack

TGA was conducted for the synthesized microcapsules containing tung oil (Figure 9). The curve demonstrated a slight mass loss starting at 250 $^{\circ}\text{C}$ followed by a significant mass loss at 350 - 480 $^{\circ}\text{C}$, at which the microcapsules ruptured and the tung oil was vaporized. This shows that the synthesized microcapsules have good thermal stability. TGA for broken microcapsules was also conducted and showed the almost exact pattern as the intact sample.

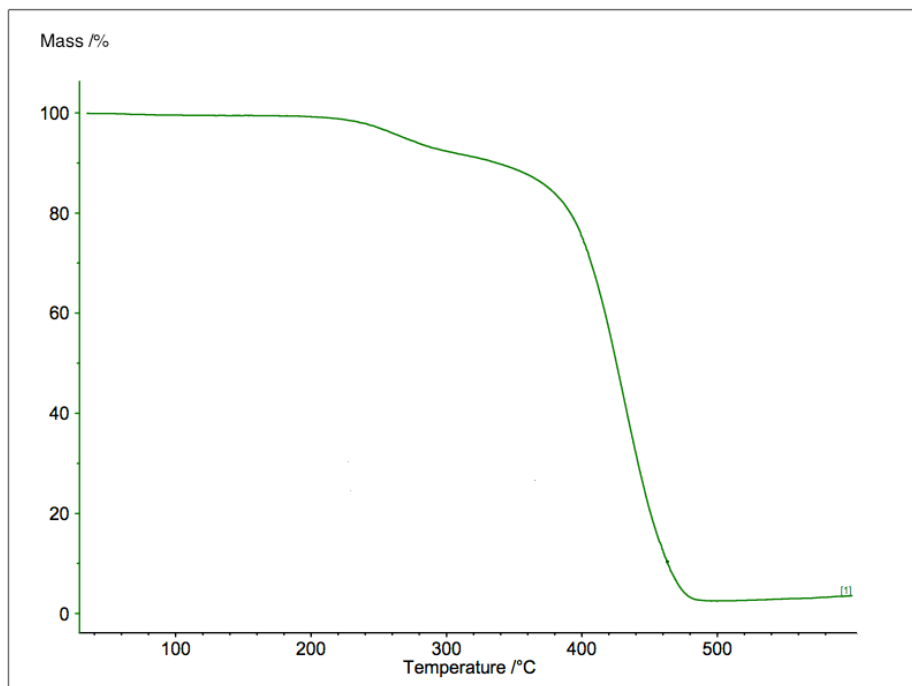


Figure 9: TGA curve of synthesized microcapsules containing tung oil

It was discovered that the size of microcapsules was significantly affected by the pH of solution. During the experiment there were several times when the pH meter was not properly calibrated, causing variations in pH. After the product was synthesized and characterized by SEM, it was realized that the size distributions of some samples made at separate times were significantly different, as mentioned above. Based on the experiment, a slight difference in pH made a large difference in microcapsule size. The largest difference in average diameter observed was 100 μm . Investigating how the size and size distribution of microcapsules affect the quality of self-healing coatings was not within the scope of this project, therefore it is strongly recommended to keep samples as similar as possible and to investigate the effect differences in microcapsule size may have in future research.

Encapsulation of 2-methylbenzothiazole

After successfully encapsulating tung oil in poly(urea formaldehyde), an attempt to encapsulate a second type of healing agent, 2-methylbenzothiazole, was performed.

With the materials already purchased for the encapsulation of tung oil, the idea of using the same procedure to encapsulate 2-methylbenzothiazole in poly(urea formaldehyde) was proposed.

The attempt to encapsulate 2-methylbenzothiazole using the tung oil procedure was not successful. This was concluded immediately upon filtering the solution when no particles were left behind on the filter paper. A possible reason for this unsuccessful encapsulation of 2-methylbenzothiazole was that the healing agent reacted with another chemical used in procedure. This hypothesis is supported by the observation of a white cloud in the emulsion solution upon addition of 2-methylbenzothiazole. Since the formaldehyde has not yet been added, the white cloud could not be poly(urea-formaldehyde). Because the unexpected reaction could not be immediately identified and the overall experiment did not produce 2-methylbenzothiazole microcapsules, this procedure was disregarded.

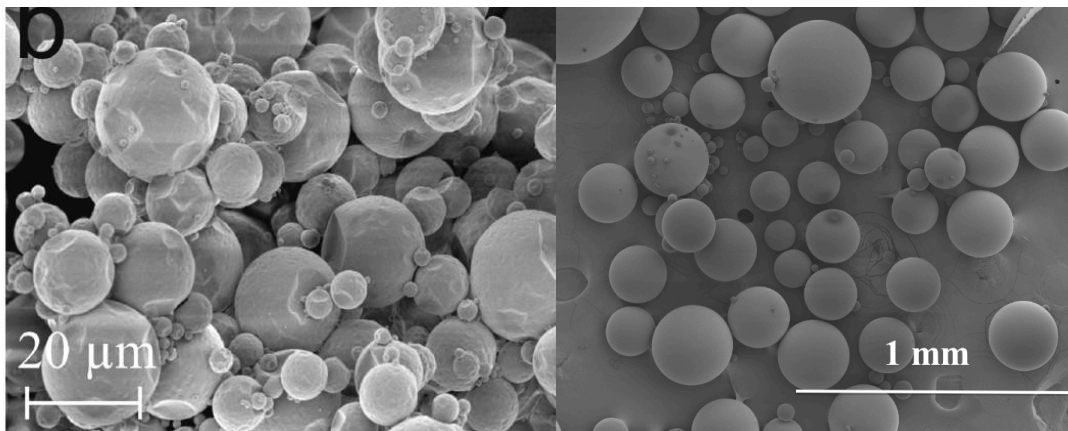


Figure 10: Encapsulation of 2-methylbenzothiazole by Latnikova *et al.* (left) and encapsulation of 2-methylbenzothiazole by MQP group (right).

Since Latnikova *et al.* successfully encapsulated 2-methylbenzothiazole in polyurea shells, this method was adopted. With a tight budget, a four propeller mechanical stirrer was used instead of the homogenizer utilized in the Latnikova *et al.*

procedure. After performing the experiment, golden spherical particles was obtained. With the naked eye, the particles seemed to look like microcapsules. Thus, SEM images of the particles were obtained as shown in Figure 10. The particles synthesized looked similar to SEM images in the literature shown in Figure 10, signifying there was a chance the particles were in fact microcapsules. To provide evidence of a successful encapsulation, a TGA experiment was performed. As shown in Figure 11, a rapid mass loss of 2-methylbenzothiazole in polyurea shells should occur at around 150 °C according to Latnikova *et al.* [27]. The TGA graph obtained on the experimental 2-methylbenzothiazole microcapsules showed no indication of a rapid mass loss at 150 °C. Therefore, this indirect evidence suggests that there was no encapsulation of 2-methylbenzothiazole in polyurea shells. Furthermore, when crushing the particles with a metal spatula, the substance refused to rupture. Thus, it was concluded that there is no encapsulated 2-methylbenzothiazole in polyurea shells.

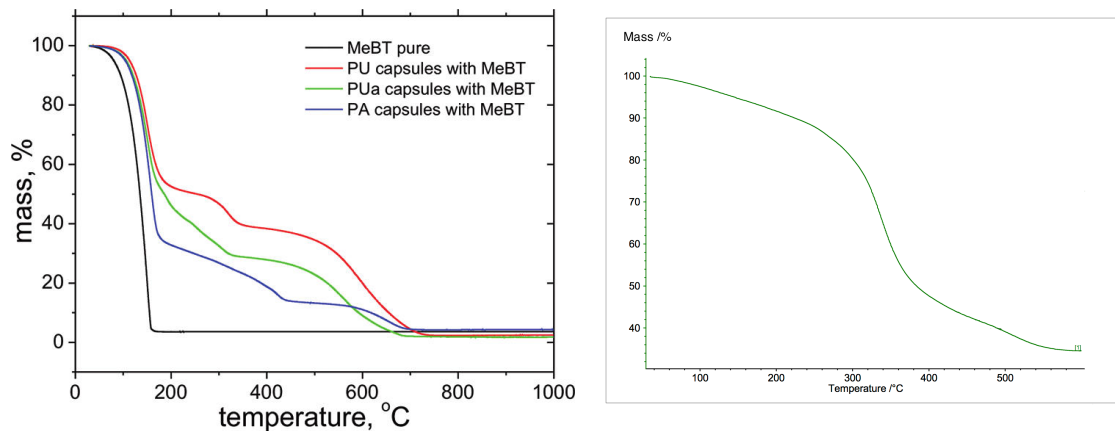


Figure 11: TGA graph of 2-methylbenzothiazole microcapsules by Latnikova *et al.* (left) and experimental TGA graph (right)

A possible reason for the failed attempt to encapsulate the healing agent may include the use of a different mixer. The procedure in the literature used a homogenizer at 17000 rpm whereas in this experiment a four impeller mechanical stirrer was used at 400

rpm. A homogenizer is a high shear mixer, which can mix highly viscous materials, whereas the mechanical stirrer is a low shear mixer. Thus, using a mechanical stirrer may not be a good choice of equipment to mix the isocyanate prepolymer, a viscous material, into the solution. Therefore, the inadequate mixing may have caused uneven distribution of prepolymer in the solution.

With limited time and resources, encapsulation of 2-methylbenzothiazole was aborted. One of the deciding factors was the expense of the materials. If 2-methylbenzothiazole was chosen as a healing agent, the cost to produce this coating in industry would be expensive. The other factor was that the materials used in the synthesis were toxic. According to New Jersey Department of Health, the chemicals such as tetraethylpentylamine used are hazardous to both humans and the environment [40]. As a result, 2-methylbenzothiazole was not investigated any further.

Preparation of Self-healing Coating Effect of Microcapsules on Epoxy Curing

During various tests of the experimental coatings, it was noted that the 10 wt.% and 20 wt.% coatings remained tacky after the unmodified epoxy had fully cured and was dry to the touch. The exact cause of this has not been determined, though several possibilities have been considered. The epoxy used consists of two parts mixed in equal proportions, which then undergo a reaction to form the solid product. It is possible that including microcapsules in the mixing process may hinder the complete mixing of the two parts which would lead to an incomplete curing. It is also possible that the tacky nature was due to some of tung oil from microcapsules ruptured during mixing and/or coating. Further testing is required to determine the exact cause and effects of this phenomenon.

Coating Thicknesses

The relative thickness of the experimental coatings as compared to the unmodified epoxy coating was considered as a potential factor for increased time to break that is unrelated to the self-healing properties of the coatings. Because the coatings are waterproof and nonconductive, increased thickness of the coating would be expected to provide more protection to the steel underneath. In order to determine if the coatings with microcapsules were thicker, several rebars were coated with the same process used in the other tests, but not encased in concrete. After the samples had cured for 72 hours, a caliper was used to measure the thickness of the rebars and coatings. A single-tailed T-test was used on the results (Figure 12) to determine if the thicknesses of the 10 wt.% and 20 wt.% coatings were significantly different from the thickness of the unmodified epoxy coating. With a confidence interval of 95%, the results of the test showed that the experimental coatings were not significantly thicker than the regular coatings.

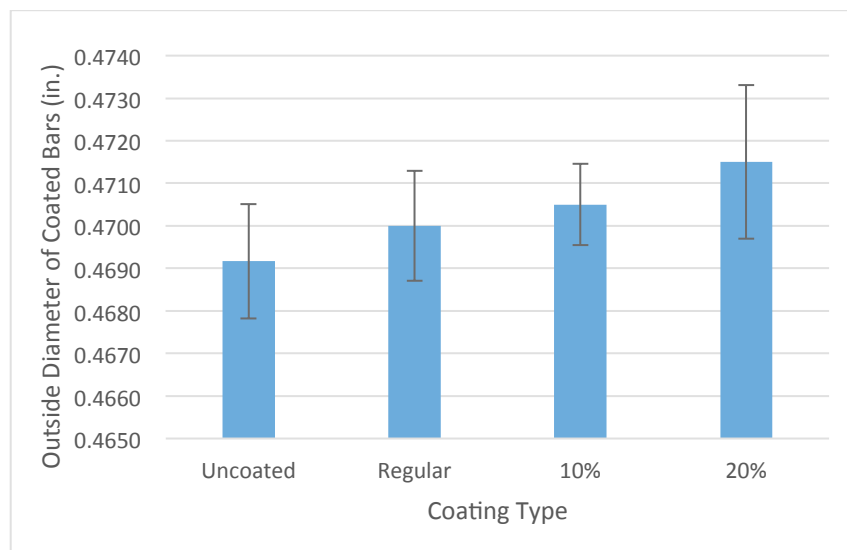


Figure 12: Outside diameter of coated rebars

Self-healing Ability

A simple test was conducted in order to confirm that the synthesized coating actually self-healed. For this test, glass slides were coated on one side with one of three

types of epoxy coating: unmodified, 10 wt.% microcapsules, and 20 wt.% microcapsules. The control and experimental samples were cut in a straight line by a brand new box cutter, and the damage was imaged using an inverted transmission optical microscope immediately, two days, five days, and seven days after the samples were cut. As shown below (Figure 13), tung oil bled out of a microcapsule and filled in the cut. This is direct evidence that tung oil is mobile enough to spread out and cover the damage when microcapsules break.

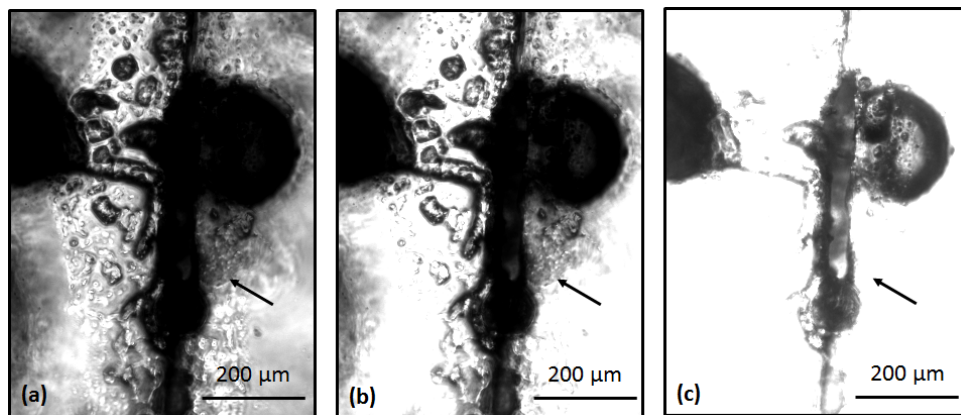


Figure 13: Optical microscope images of tung oil bleeding out of a microcapsule under (a) low, (b) medium, and (c) high exposure (10 wt.%, 5 days after damage)

Additionally, there was a newly formed film of oxidized tung oil observed in the vicinity of the damage. Five days after the samples with 10 and 20 wt.% microcapsules were damaged, a band with rough texture was formed all the way along the straight cut. As shown in Figure 14 (b), this band has a very different texture from the original coating. This band resulted from the oxidized tung oil, because it did not exist immediately after the sample was damaged, based on Figure 14 (c). Figure 14 (d) shows a band formed near a cut microcapsule. This band was also observed in the sample two days after being cut, but the band was only formed near broken microcapsules and hadn't completely spread along the cut. This concluded that the synthesized coatings do self-heal and take a few days to repair damage.

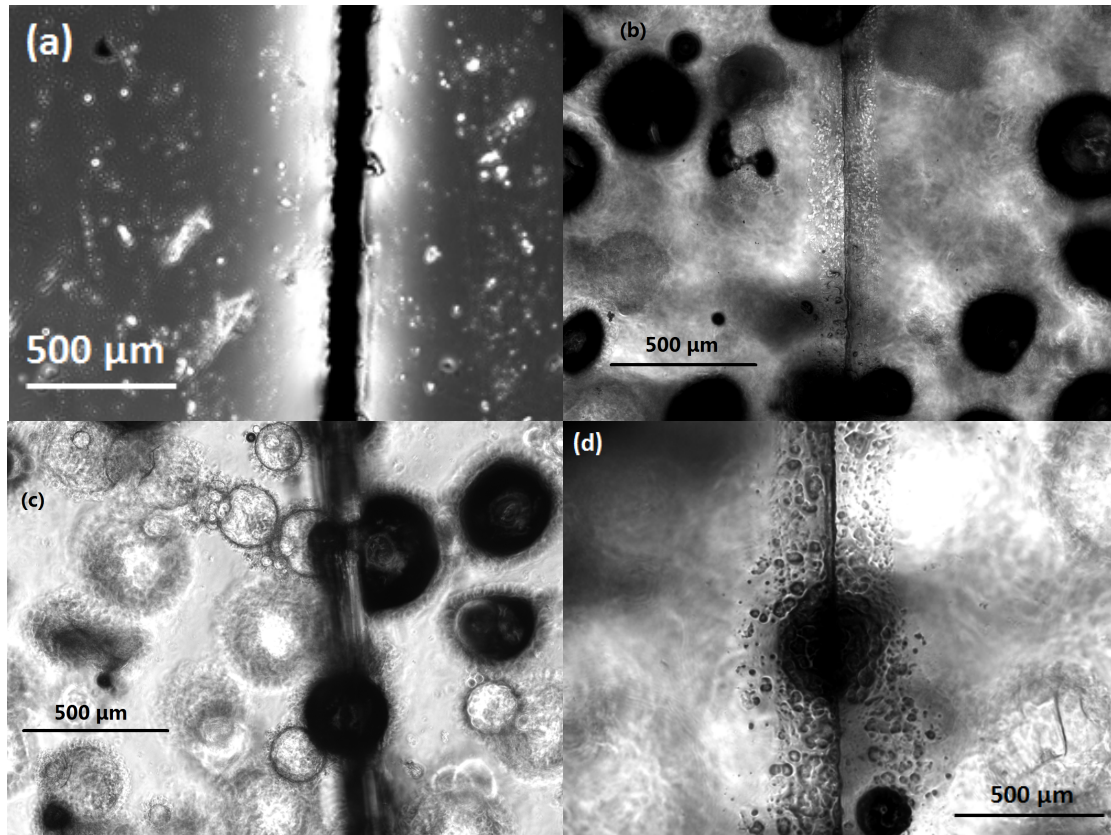


Figure 14: Optical microscope images of cuts made on samples. (a) A cut made on unmodified epoxy coating; (b) a cut made after 5 days on the sample with 20 wt.% microcapsules; (c) a cut made immediately on the sample with 20 wt.% microcapsules; (d) a close up image of a microcapsule (5 days)

Concrete Mix Design

Sieve Analysis

A sieve analysis was completed on the fine aggregate used to make the samples. The analysis determined the distribution of particle sizes within the sand used. This test was done for quality control reasons and the results of three separate sieve analyses on the aggregate netted the results shown in the appendix (Figure 33). As shown in Figure 15, the experimental results do not fall between the upper and lower industry standard limits. Even though the aggregate used in the samples for accelerated corrosion testing and pullout testing was not at industry standards, this should not impact analysis of the results significantly because the same aggregate was used throughout the experiments. The relative differences and effects can still be observed.

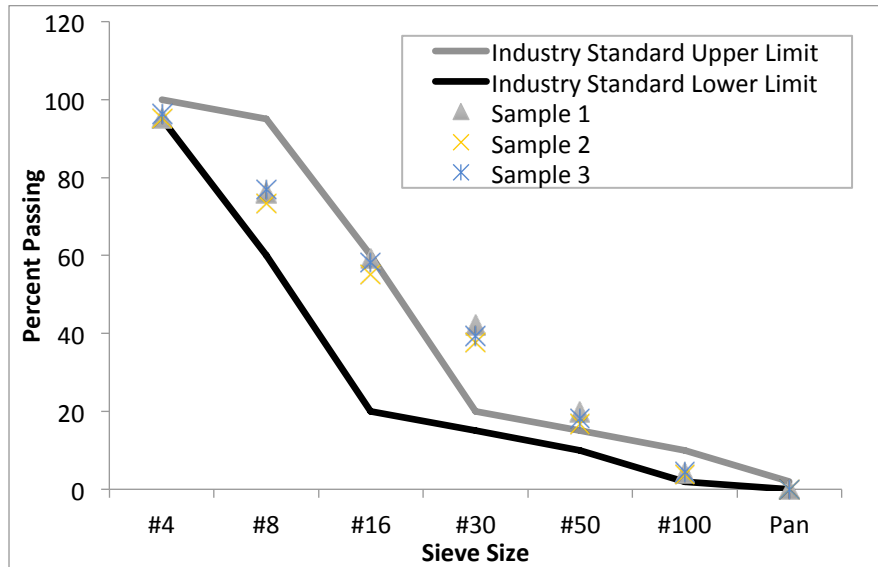


Figure 15: Sieve analysis results of aggregate

Compression Testing

Compression testing was performed on several samples as a measure of quality control. The test involved crushing 2” cubes of concrete in the universal testing machine at various days during the curing process. The samples were tested after 1, 7, and 28 days in accordance with industry standard. The results of this testing (Figure 16) showed that the mix design used meets the industry standard 28 day compression strength of approximately 6000 psi.

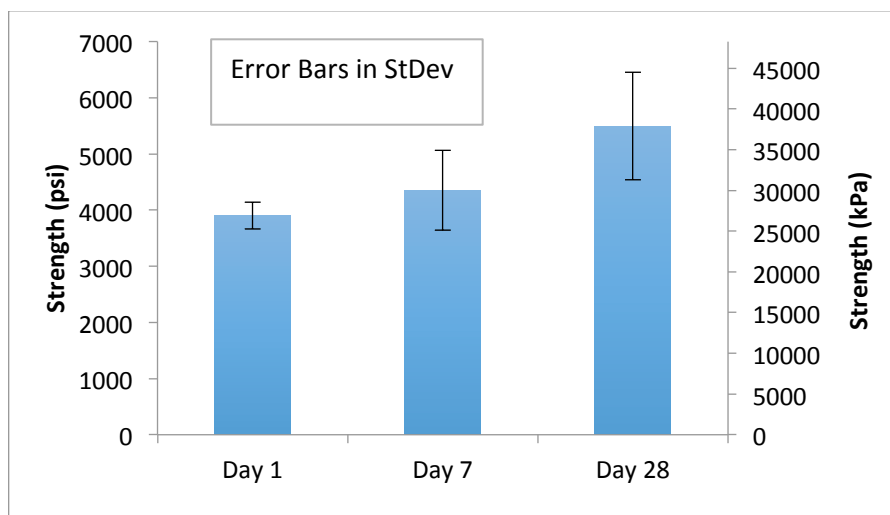


Figure 16: Graph of the peak strengths on various days of the compression tests

Pullout Testing

The results of the rebar pullout tests (Figure 17) showed only minor differences in the pullout strength for each of the four coating types tested. The peak loads for the samples with no coating, unmodified epoxy coating, and epoxy coating with 20 wt.% microcapsules all showed significantly overlapping standard deviations. The standard deviations of these samples are relatively large, which is due in part to both the sensitive nature of the test and the low number of samples per experimental group. This precludes any absolute determinations on the relative pullout strengths of these samples. However, the 10 wt.% coating does show lower pullout strength. Further testing in the future and a review of the precision of sample creation will likely provide valuable information on this aspect of the coatings. One of the broken samples was shown as Figure 18.

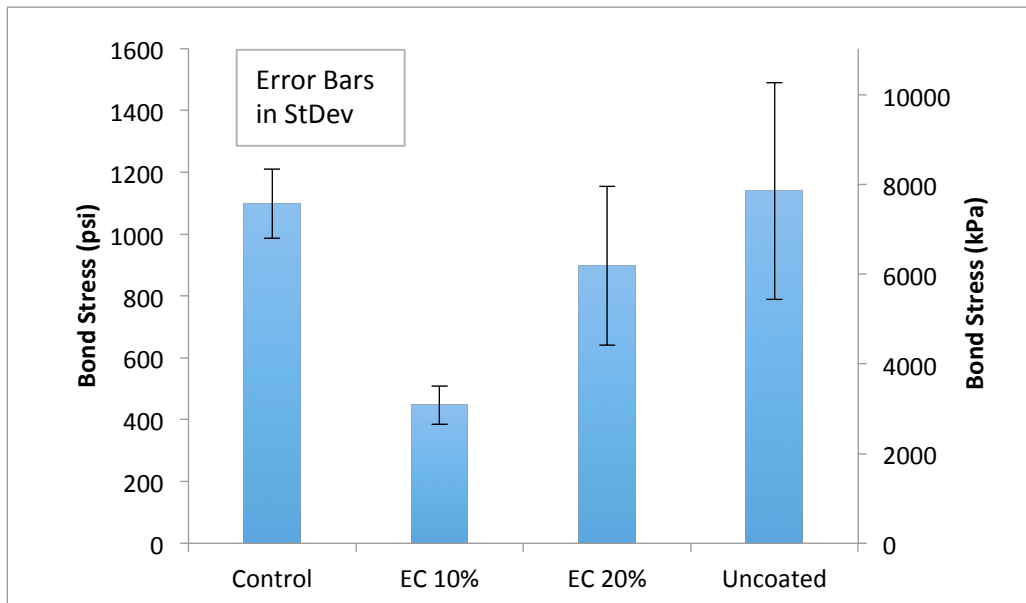


Figure 17: Graph of the peak strengths on various days of the pullout test



Figure 18: A broken sample by pullout testing coated with self-healing coating with 20 wt.% microcapsules

Accelerated Corrosion Testing

Through the accelerated corrosion testing it was determined that our experimental coating had a substantial and positive effect on inhibiting corrosion. The unmodified epoxy coating lasted an average of 11.5 +/- 3.5 days and the damaged unmodified epoxy coating an average of 13 +/- 5 days, as illustrated in Figure 19 below. The experimental coatings, which included either 10 wt.% or 20% microcapsules by weight, took at least three times longer to break. There were no significant differences in the damaged vs. undamaged samples tested. This could possibly be due to the damage not being large enough to impact the results. As of this writing the experimental coatings have only had 3 failures of the 12 total samples, which occurred at days 47, 58, and 74. The 10 wt.% and 20 wt.% microcapsule coatings tested have not yet had any significant statistical differences between them.

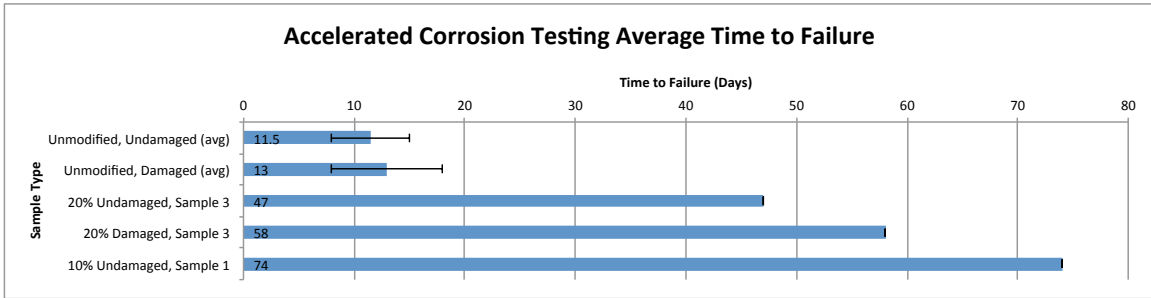


Figure 19: Failure time for accelerated corrosion test

The first experimental sample that failed only showed minor cracking of the concrete, but it was determined to have failed by concrete cracking via the recorded decrease in resistance. The spike in voltage through the sample can be seen in Figure 20 below, peaking at day 60 when the sample was removed from testing due to failure. The minor damage is likely due to the short amount of time between the initial failure and the end of testing for that sample. Once the voltage first spikes, the sample is considered failed. Any data after that is unnecessary, and allowing the samples to continue to degrade for too long runs a risk of burning out the circuit.

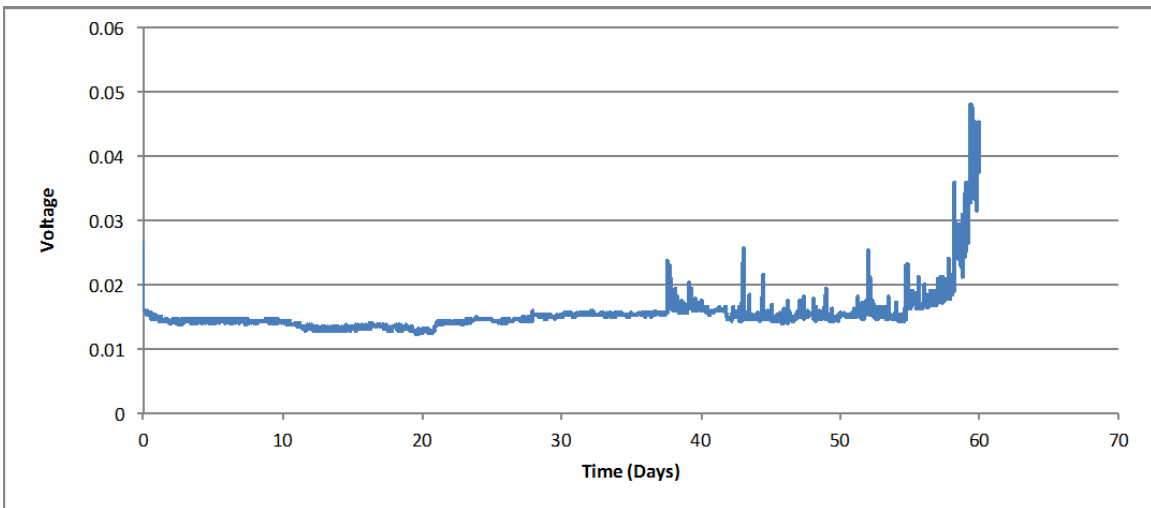


Figure 20: Voltage with respect to time for 20 wt.% damaged in accelerated corrosion test



Figure 21: One of the corroded samples for unmodified epoxy coating

Conclusions

Self-healing coatings were prepared by incorporating microcapsules containing tung oil, which were synthesized by an oil-in-water emulsion process, into conventional epoxy coatings. This advanced coating considerably enhanced anti-corrosion performance of rebar during accelerated corrosion testing. This result shows the potential to extend the service life of concrete reinforcement by at least 300% as compared to unmodified conventional epoxy coatings. Self-healing coatings also showed no significant decrease in pullout strength from concrete when 20 wt.% of microcapsules were incorporated. Therefore, the self-healing coatings developed by this project are superior to unmodified conventional epoxy coatings in producing more durable concrete structures.

Performance differences between the samples with damaged and undamaged coatings were not observed in this project, most likely because the damage made to the self-healing coatings was not severe enough. In order to investigate the capability of self-healing coatings to prolong the service life of damaged concrete structures, it is suggested to induce damages in a better way.

There are numerous avenues for future research in this area. The microcapsule size, which was significantly affected by the pH of the solution during synthesis, was not strictly controlled, and the effect of microcapsule's size on the performance of self-healing coating should be investigated. Additionally, while initial testing showed that the proportion of microcapsules included did not significantly affect the coating thickness, further testing should be conducted to confirm this. Furthermore, whether it is feasible to encapsulate 2-methylbenzothiazole for self-healing coating needs further investigations as cost and time constraints prevented additional attempts by this team.

Appendix A

Synthesis of Microcapsules

Tung oil-microcapsules used in accelerated corrosion test:

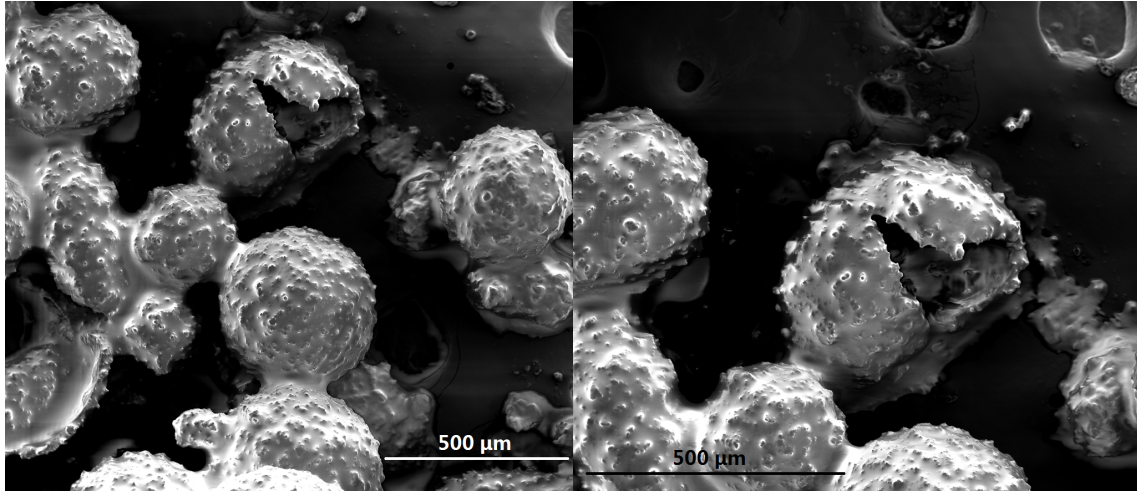


Figure 22: SEM images of microcapsules containing tung oil from one of the batches

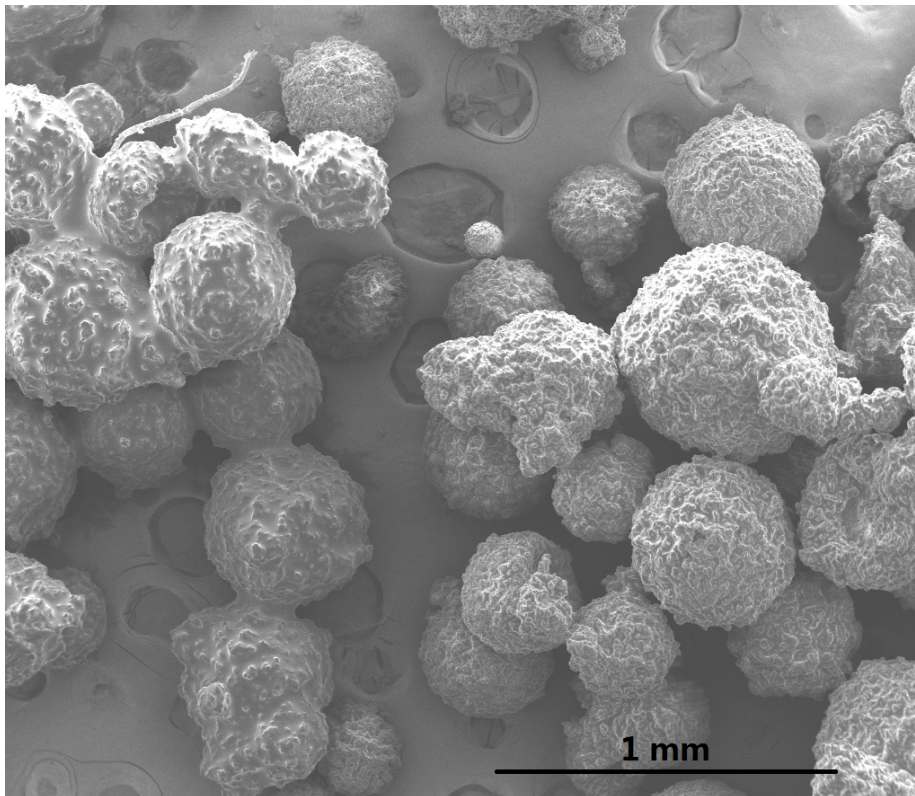


Figure 23: SEM images of microcapsules containing tung oil from a different batch

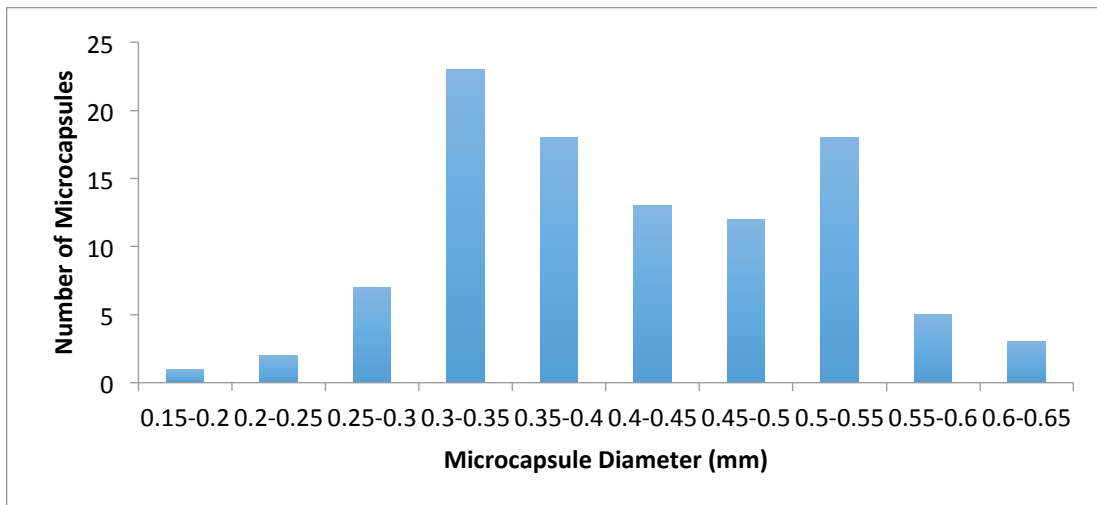


Figure 24: Size distribution of tung oil microcapsules

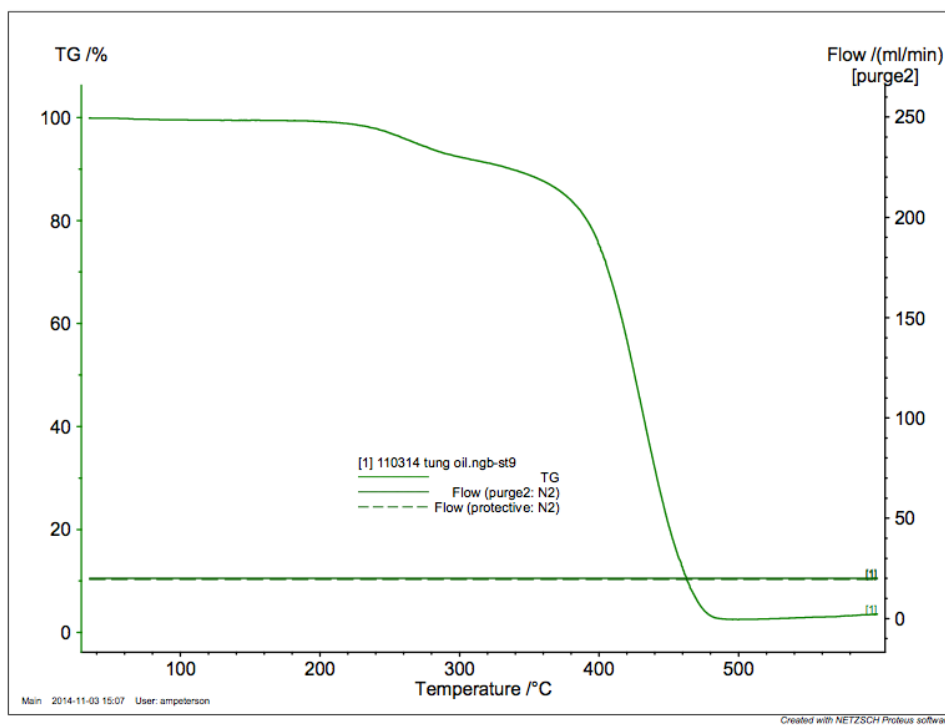


Figure 25: Thermalgravimetric Analysis of encapsulated tung oil over temperature

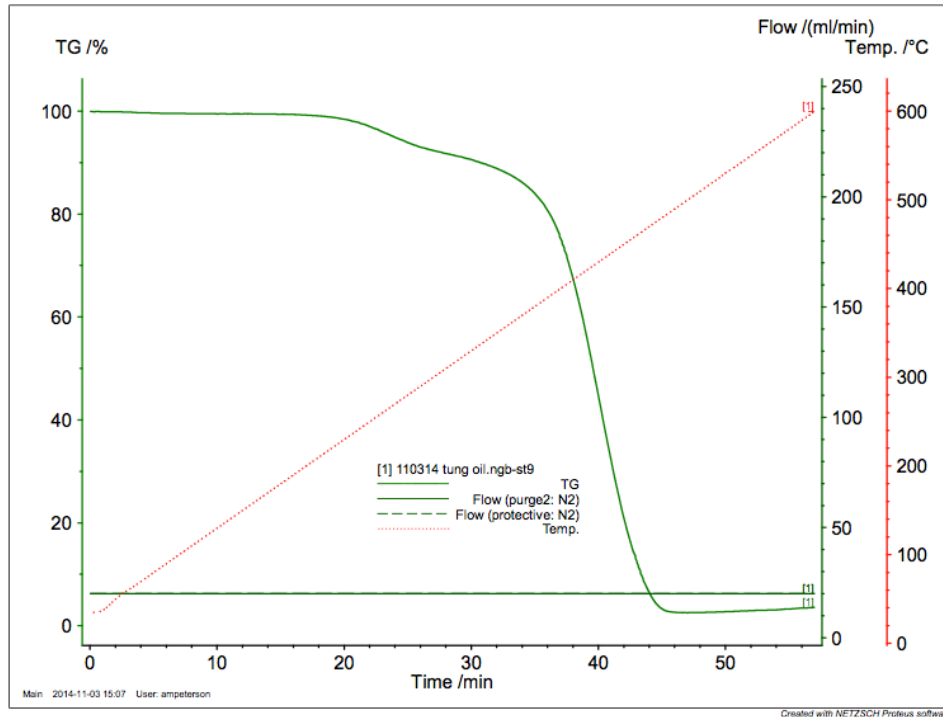


Figure 26: Thermalgravimetric Analysis of encapsulated tung oil over time

Tung Oil- microcapsules used in thickness test:

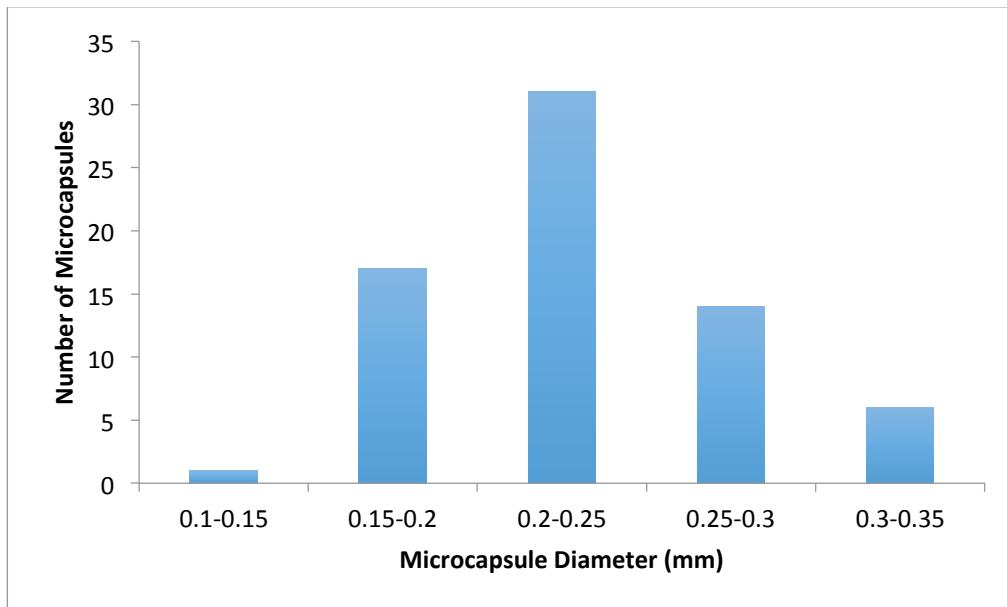


Figure 27: Size distribution of tung oil microcapsules

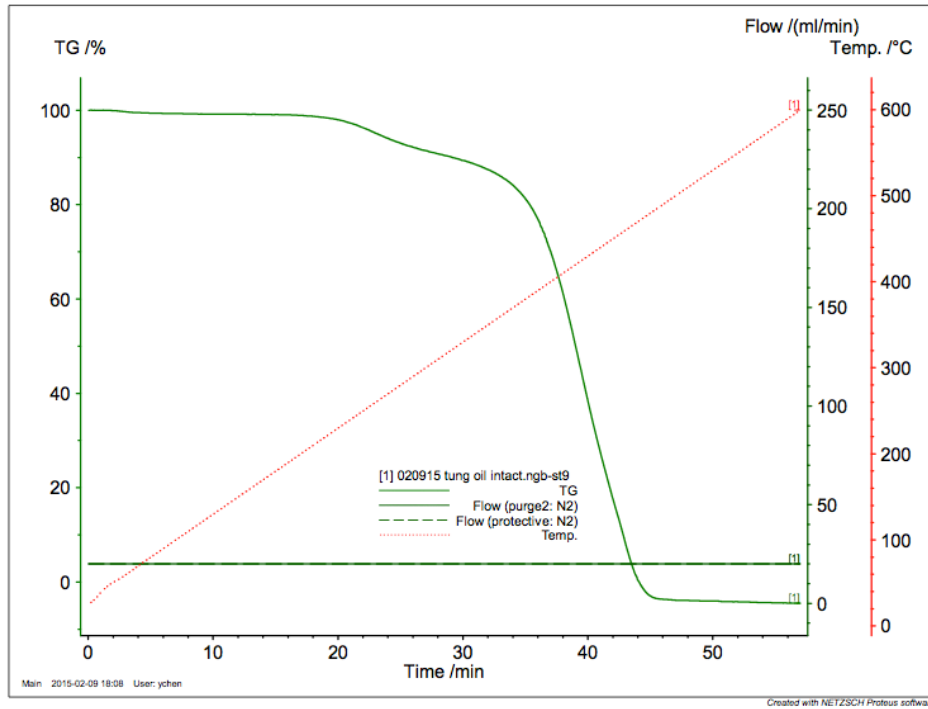


Figure 28: Thermalgravimetric Analysis of encapsulated tung oil over temperature

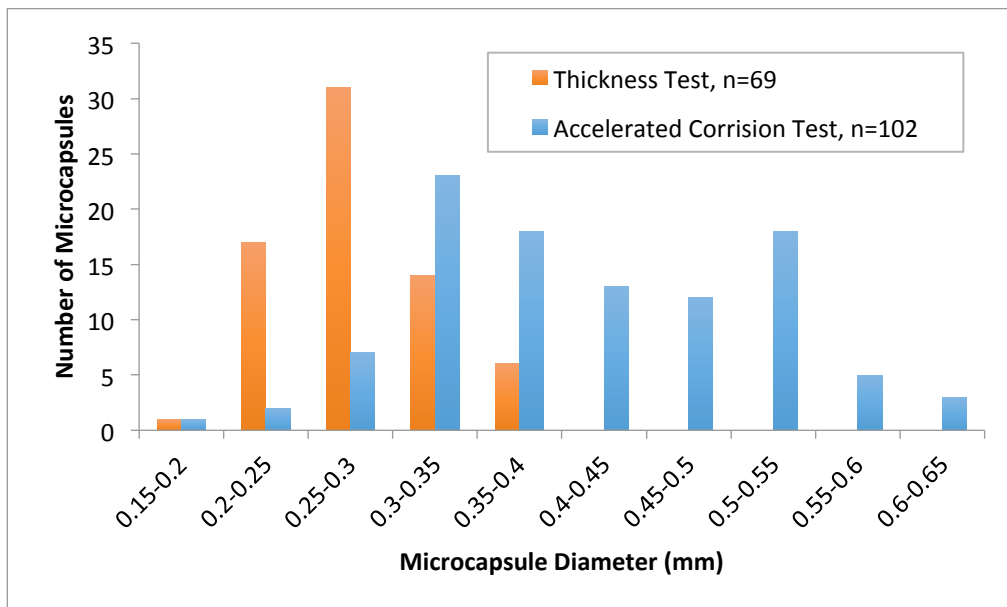


Figure 29: Comparison of the microcapsules size for the thickness test and the microcapsule size for the accelerated corrosion test.

2-Methylbenzothiazole - failed attempt:

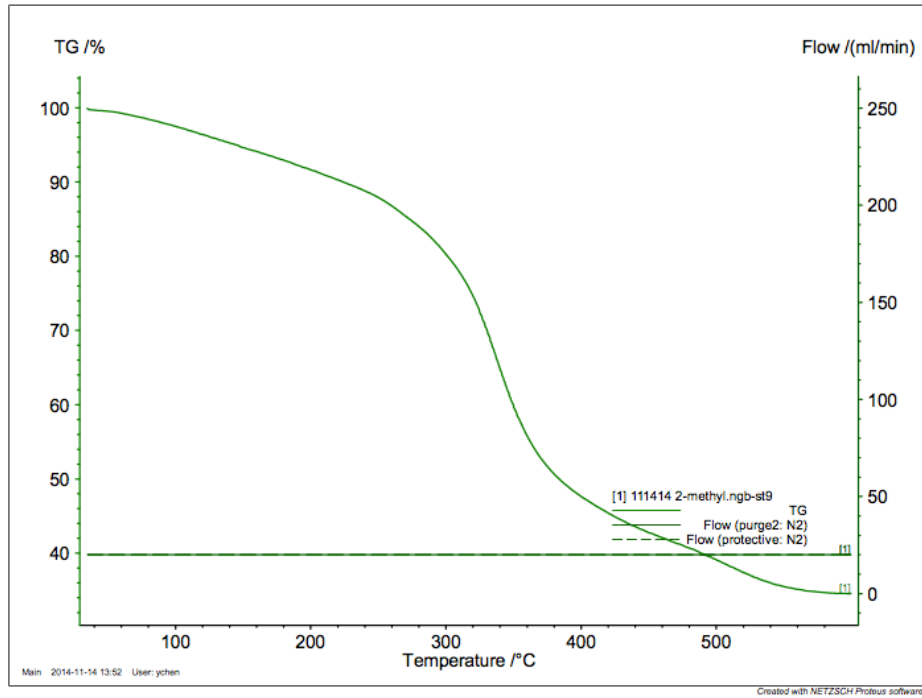


Figure 30: Thermalgravimetric Analysis of the attempt to encapsulate 2-methylbenzothiazole over temperature

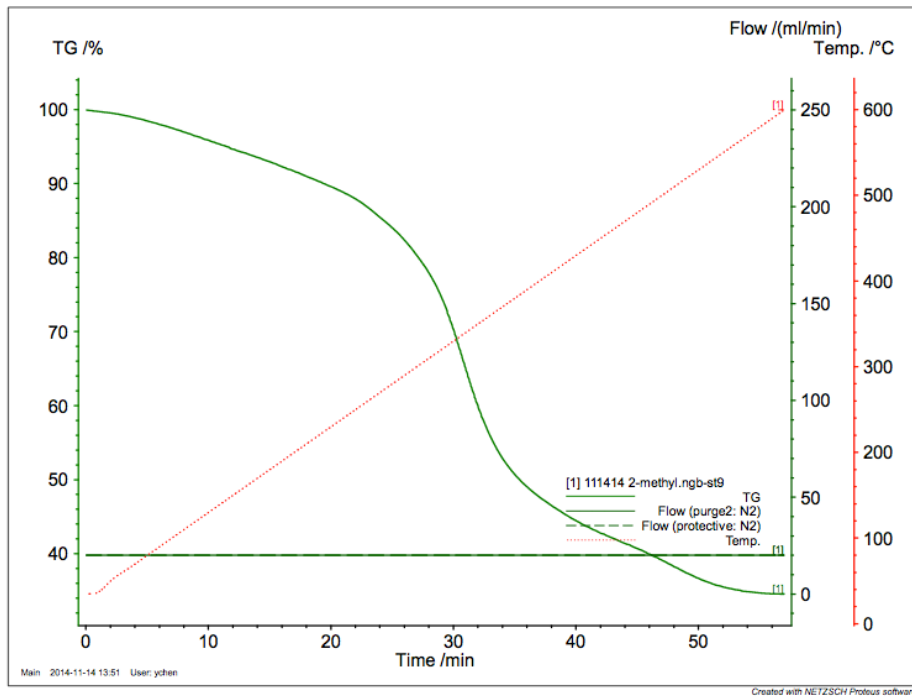


Figure 31: Thermalgravimetric Analysis of the attempt to encapsulate 2-methylbenzothiazole over time

Appendix B
Quality Test
Sieve Analysis

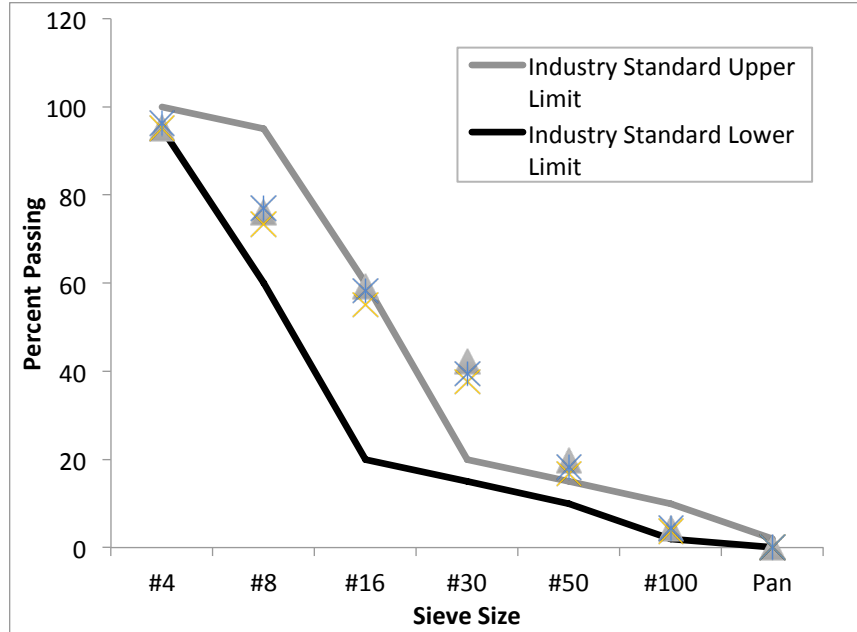


Figure 32: Graduation Chart for comparison of industry standard and experimental aggregate

Fine Aggregate		ASTM Spec C136			
Sieve Size	Upper Limit % Passing	Lower Limit % Passing	Sample 1 % Passing	Sample 2 % Passing	Sample 3 % Passing
#4	100	95	95.15	95.24	96.27
#8	95	60	76.05	73.34	76.96
#16	60	20	59.27	55.07	58.24
#30	20	15	42.22	37.65	39.44
#50	15	10	19.79	16.7	18.15
#100	10	2	4.22	3.72	4.41
Pan	2	0	0	0	0

Figure 33: Table of percent passing industry standard and experimental aggregate

Pullout Testing

	Bond Stress (psi)			
	Reg EC	EC 10%	EC 20%	Uncoated
Sample 1	1132	436	779	1084
Sample 2	973	549	723	820
Sample 3	1189	447	1193	1516
Avg	1098	447	898	1140
StDv	112	62	257	351
StDv/avg	0.102	0.139	0.286	0.308

Figure 34: Table of the peak stresses of the pullout test

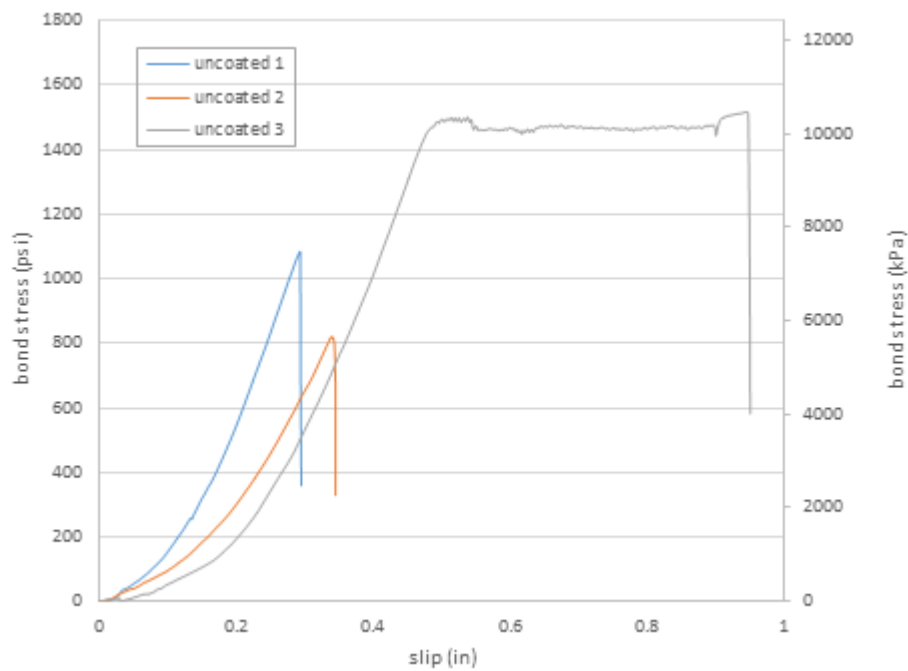


Figure 35: Pullout graphs of the uncoated samples

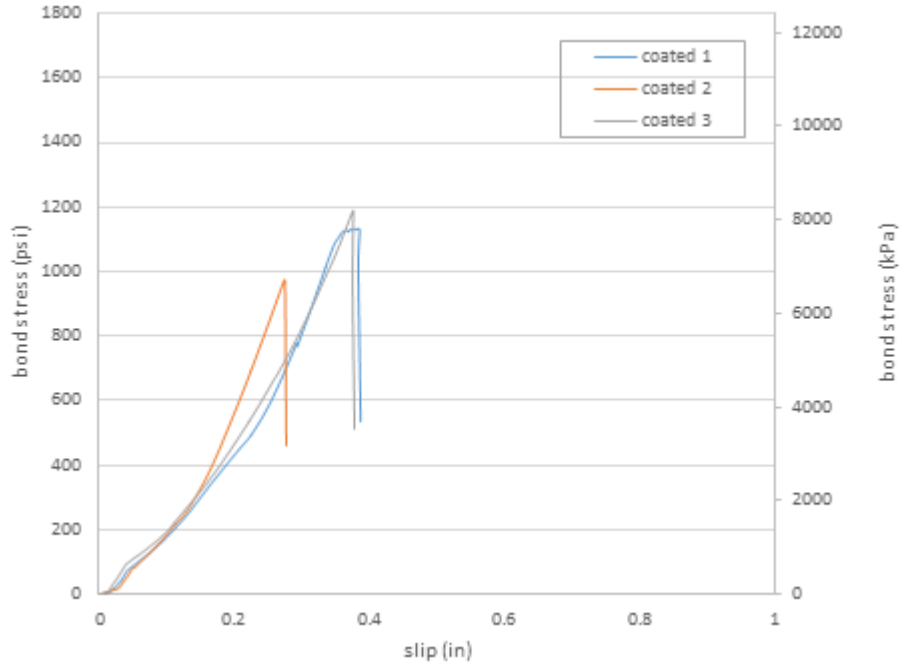


Figure 36: Pullout graphs of the regular coated samples

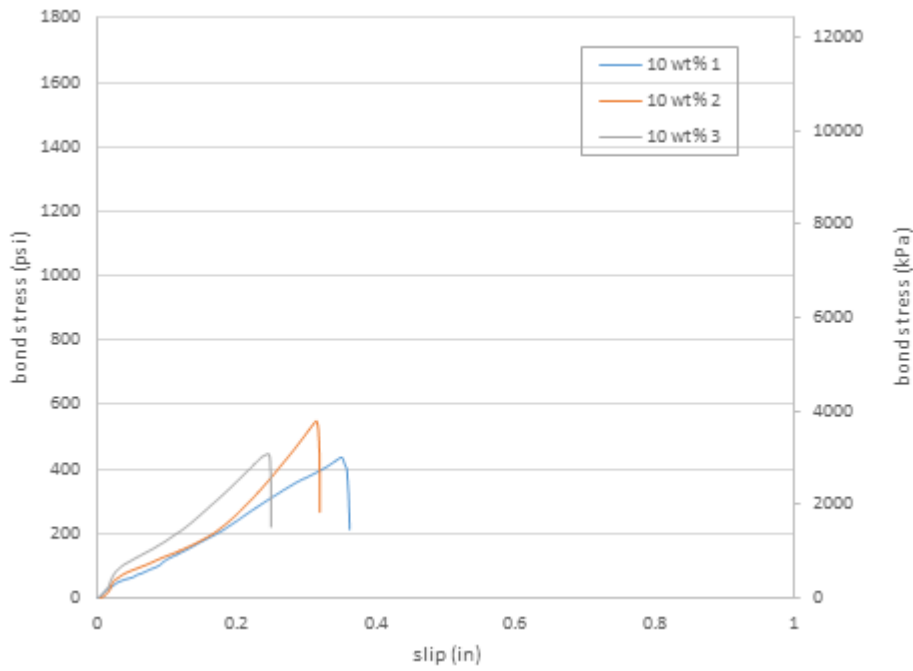


Figure 37: Pullout graphs of the 10 wt.% tung oil EC samples

Note: Sample 10 wt.% 1 had a slip of about 0.24 in at the beginning of test. This was accounted for which is why all the samples started at 0 inches of slip.

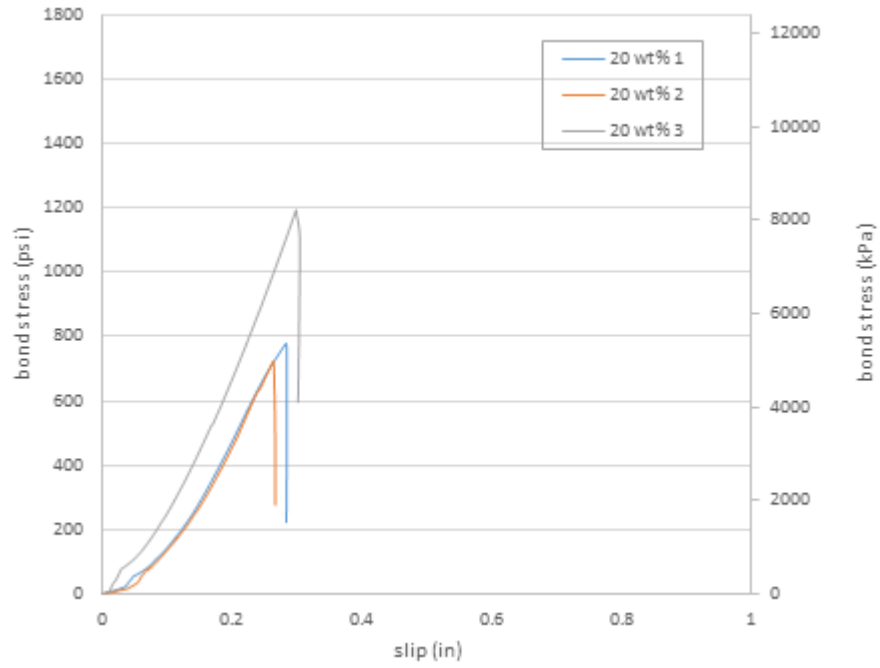


Figure 38: Pullout graphs of the 20 wt.% tung oil EC samples

Compression Test

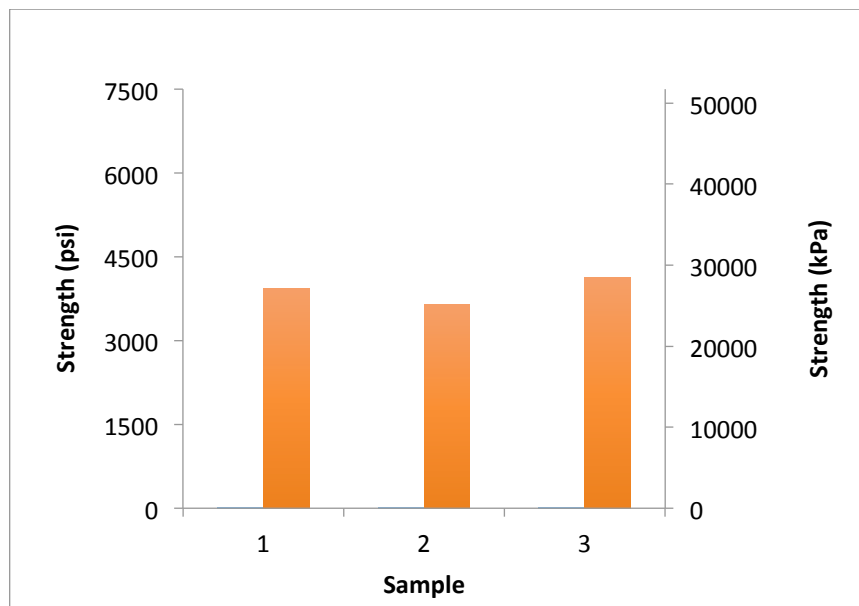


Figure 39: Compression test of day 1 peak strengths

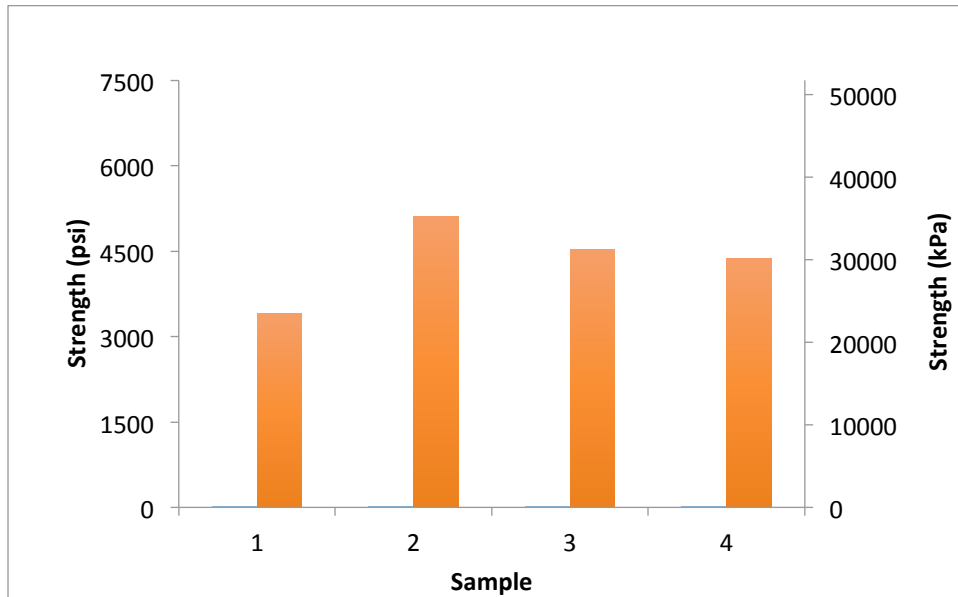


Figure 40: Compression test of day 7 peak strengths

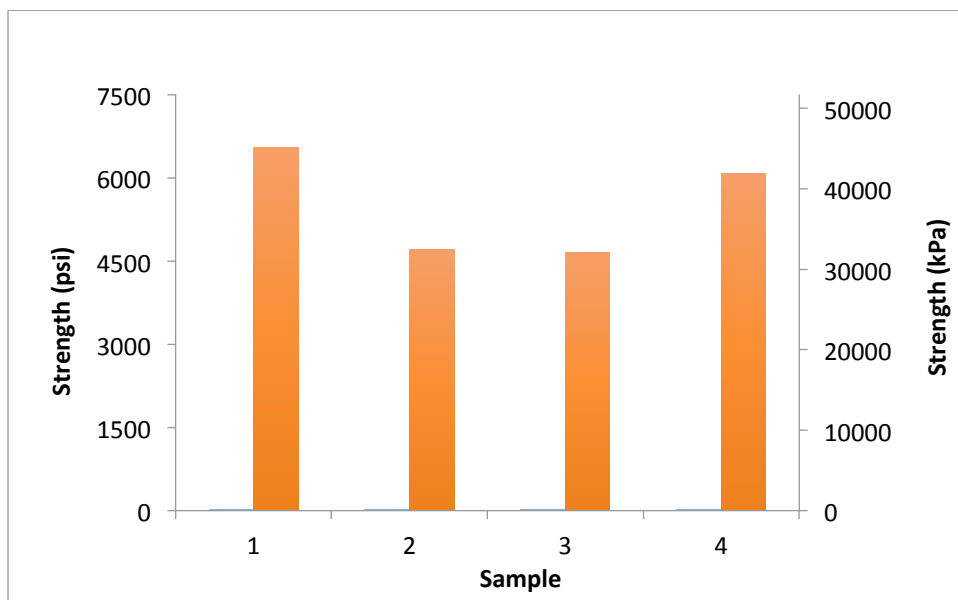


Figure 41: Compression test of day 28 peak strengths

Thickness Test

Coating Type	Outside Diameter (in.)					
	Sample 1	Sample 2	Sample 3	Sample 4	Sample 5	Sample 6
Uncoated	0.470	0.471	0.470	0.469	0.467	0.468
Regular	0.472	0.470	0.469	0.471	0.470	0.468
10%	0.470	0.471	0.472	0.471	0.470	0.469
20%	0.471	0.471	0.469	0.471	0.472	0.475

Figure 42: Statistics for coating thickness measurement

Coating Type	Average	Avg. Coating Thickness (in)	Standard Deviation
Uncoated	0.469	0.0000	0.0013
Regular	0.470	0.0004	0.0013
10%	0.471	0.0007	0.0010
20%	0.472	0.0012	0.0018

Figure 43: Average for coating thickness measurement

Appendix C

Accelerated Corrosion Test

Regular Coating Trial 1:

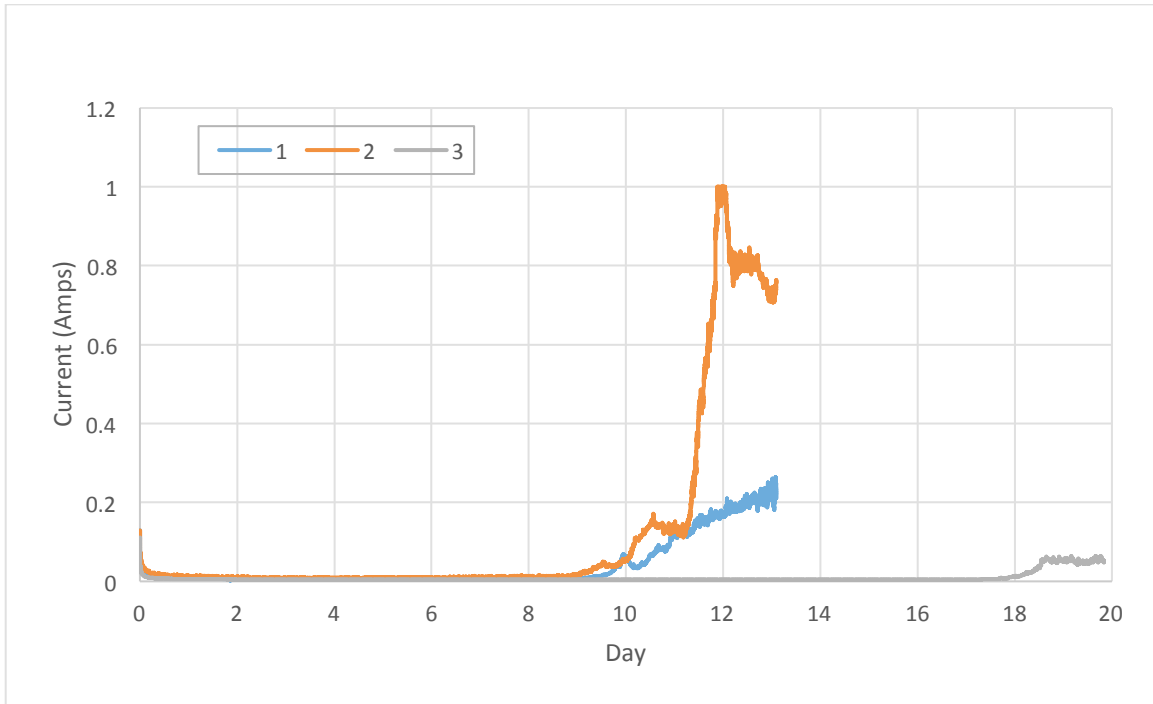


Figure 44: Graph of current with time of regular coating undamaged

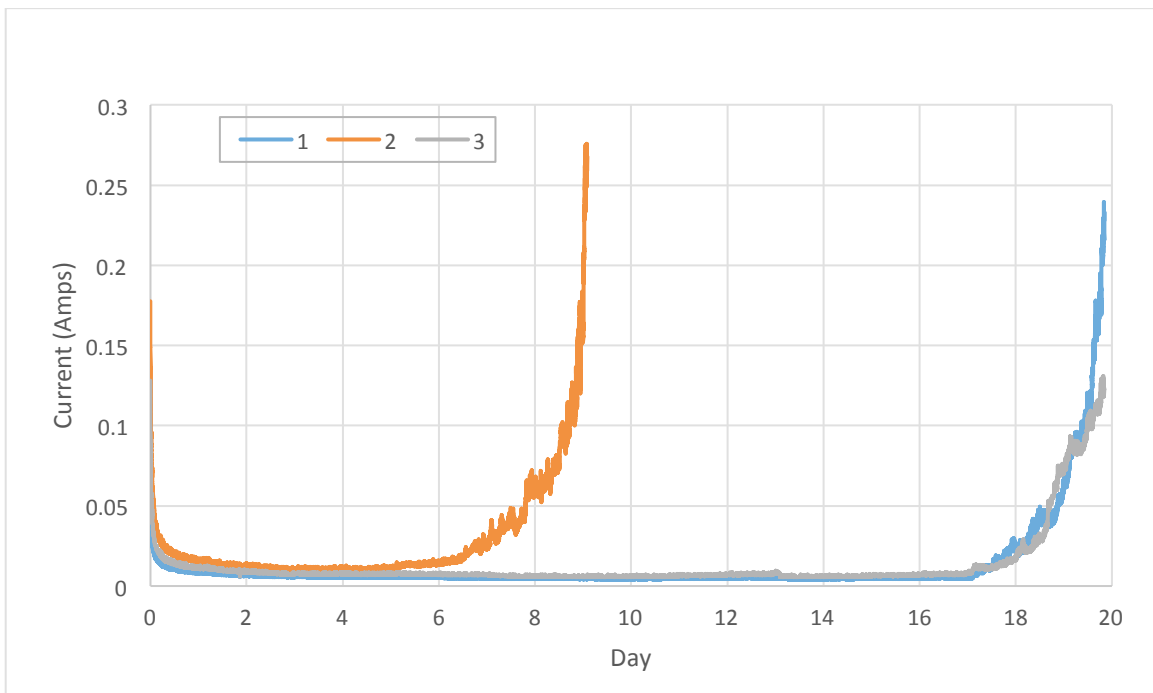


Figure 45: Graph of current with time of regular coating damaged

Civil Engineering Design Statement

The design problem for this project was to develop a process for incorporating microcapsules of a healing agent into a coating for steel rebar, then apply various tests in order to determine both the effectiveness of the healing agent and the applicability to solving current infrastructure maintenance problems. The primary testing involved accelerated corrosion testing to determine the relative lifespan of the experimental coatings as compared to industry standard epoxy coatings. Additional testing was performed to test the pullout strength and relative thickness of the coating to investigate any possible effect on a structure's strength. Assembling this information allows for a proper assessment of whether or not this coating is beneficial based on its relative improvements and costs.

Professional Licensure Statement

Professional licensure for the field of civil engineering is the process of obtaining a professional engineers license. This license is regulated by individual states in order to protect the residents of the state.

In order to obtain a professional engineer license an individual must take a (FE) Fundamentals of Engineering exam. Once this is passed the individual is designated an Engineer in-Training. They must then work in their desired field of engineering, under a professional engineer for 4 years before taking the (PE) Professional Engineers exam. The individual can then apply for the license through the state they reside in.

Obtaining a PE license is beneficial to the public, the engineer, and the profession for many reasons. When an individual obtains a PE license it is a guarantee to the public of the area that they are working that they had the required background and education to safely perform their role in society. This license and licensure process is beneficial to the individual going through this process because it shows that they are dedicated to the profession and they are willing to invest time in the profession. The profession also benefits greatly from the aforementioned reasons due to the individuals being dedicated to the profession.

References

1. 2013 Report Card for America's Infrastructure.
<http://www.infrastructurereportcard.org/> (accessed 9/6/2014).
2. Status of the Nation's Highways, Bridges, and Transit: Conditions & Performance.
<http://www.fhwa.dot.gov/policy/2010cpr/> (accessed 9/6/2014).
3. NASA, Corrosion Technology Laboratory: Why Metals Corrode.
4. *Britannica, E.*, Steel. Encyclopædia Britannica Inc.
5. Gräfen, H.; Horn, E.-M.; Schlecker, H.; Schindler, H., Corrosion. In Ullmann's Encyclopedia of Industrial Chemistry, Wiley-VCH Verlag GmbH & Co. KGaA: 2000.
6. Ball, J. C., Electrochemical Treatment: Extending the Life of a Historic Viaduct Structure. *Structure Magazine*, 2007.
7. Soylev, T. A.; François, R., *Cement and Concrete Research* **2003**, 33 (9), 1407-1415.
8. Chen, G.; Volz, J.; Brow, R.; Yan, D.; Reis, S.; Wu, C.; Tang, F.; Werner, C.; Tao, X., Coated Steel Rebar for Enhanced Concrete-Steel Bond Strength and Corrosion Resistance. Missouri University of Science and Technology: Rolla, MO, 2010.
9. Development of hexavalent chromium-free corrosion protection layers on surface. *Advanced Coatings & Surface Technology* 2012/05//, 2012, p 9.
10. JF. García, S. J.; Fischer, H. R.; van Der Zwaag, S., *Progress in Organic Coatings* **2011**, 72 (3), 211-221.
11. Khramov, A. N.; Voevodin, N. N.; Balbyshev, V. N.; Donley, M. S., *Thin Solid Films* 2004, 447-448 (0), 549-557.
12. Zheludkevich, M. L.; Salvado, I. M.; Ferreira, M. G. S., *Journal of Materials*

- Chemistry 2005, 15 (48), 5099-5111.
13. Fritz, J. D.; Grubb, J. F.; Polinski, R. F., *Advanced Materials & Processes* **2001**, 159, 36.
 14. Mahmoud, K. M., *Innovations in Bridge Engineering Technology*. T&F Books UK: 2009.
 15. Hansen, A.; Furman, A.; Hansen, M.; Green, A.; Meyer, J., *Galvanic Liquid Applied Coating for the Protection of Concrete Reinforcement*. NACE International: White Bear Lake, MN, 2008.
 16. Reinforcing Steel. <http://www.crsi.org/index.cfm/steel/about> (accessed 9/19/2014).
 17. Yeih, W.; Huang, R.; Chang, J. J.; Yang, C. C., *Advanced Cement Based Materials* **1997**, 5 (2), 57-65.
 18. Jorge, S.; Dias-da-Costa, D.; Júlio, E., *Engineering Structures* **2012**, 36, 372-378.
 19. Okba, S. H.; El-Dieb, A. S.; Reda, M. M., *Cement and Concrete Research* **1997**, 27 (6), 861-868.
 20. Ohama, Y., *Handbook of Polymer-Modified Concrete and Mortars - Properties and Process Technology*. 1995.
 21. Manning, D. G., *Construction and Building Materials* **1996**, 10 (5), 349-365.
 22. Brown, E. N.; Kessler, M. R.; Sottos, N. R.; White, S. R., *Journal of Microencapsulation* 2003, 20 (6), 719-730.
 23. Finšgar, M.; Milošev, I., *Corrosion Science* **2010**, 52 (9), 2737-2749.
 24. Sun, W.; Wang, L.; Wu, T.; Liu, G., *Corrosion Science* **2014**, 82 (0), 1-6.
 25. Borisova, D.; Möhwald, H.; Shchukin, D. G., *ACS nano* **2011**, 5 (3), 1939-1946.
 26. Abdullayev, E.; Price, R.; Shchukin, D.; Lvov, Y., *ACS applied materials &*

- interfaces* **2009**, *1* (7), 1437-1443.
27. Latnikova, A., Capsules Made of Cross-Linked Polymers and Liquid Core: Possible Morphologies and Their Estimation on the Basis of Hansen Solubility Parameters.
 28. Peterson, A. M.; Jensen, R. E.; Palmese, G. R., *ACS applied materials & interfaces* **2009**, *1* (5), 992-995.
 29. Peterson, A. M.; Jensen, R. E.; Palmese, G. R., *ACS applied materials & interfaces* **2010**, *2* (4), 1141-1149.
 30. Pratama, P. A.; Peterson, A. M.; Palmese, G. R., *Macromolecular Chemistry and Physics* **2012**, *213* (2), 173-181.
 31. Peterson, A. M.; Jensen, R. E.; Palmese, G. R., *ACS applied materials & interfaces* **2013**, *5* (3), 815-821.
 32. Peterson, A. M.; Palmese, G. R., *Macromolecular Chemistry and Physics* **2013**, *214* (16), 1798-1805.
 33. Pratama, P. A.; Sharifi, M.; Peterson, A. M.; Palmese, G. R., *ACS applied materials & interfaces* **2013**, *5* (23), 12425-12431.
 34. Suryanarayana, C.; Rao, K. C.; Kumar, D., *Progress in Organic Coatings* **2008**, *63* (1), 72-78.
 35. Jadhav, R. S.; Hundiwale, D. G.; Mahulikar, P. P., *Journal of applied polymer science* **2011**, *119* (5), 2911-2916.
 36. Samadzadeh, M.; Boura, S. H.; Peikari, M.; Ashrafi, A.; Kasiriha, M., *Progress in Organic Coatings* **2011**, *70* (4), 383-387.
 37. Hatami Boura, S.; Peikari, M.; Ashrafi, A.; Samadzadeh, M., *Progress in Organic*

- Coatings* **2012**, 75 (4), 292-300.
38. Chen, Y.; Jiang, Y. Y.; Chen, H.; Zhang, Z.; Zhang, J. Q.; Cao, C. N., *Journal of the American Oil Chemists' Society* **2013**, 90 (9), 1387-1395.
39. Ahmad, S., *Arabian Journal for Science and Engineering* **2009**, 34 (2), 95.
40. *Hazardous Substance Fact Sheet*. Trenton, NJ: Dept., 2010. Web. 23 Feb. 2015.